AD-A253 270

TECHNICAL REPORT BRL-TR-3381

BRL

NUMERICAL EXPERIMENTS ON ADIABATIC SHEAR BAND FORMATION IN ONE DIMENSION

JOHN W. WALTER, JR.

JULY 1992

U.S. ARMY LABORATORY COMMAND

BALLISTIC RESEARCH LABORATORY
ABERDEEN PROVING GROUND, MARYLAND

92 7 27 193

92-20272

NOTICES

REPORT DOCUMENTATION PAGE

Public reporting burden for this collection of information is estimated to average 1 hour per response, including the time for reviewing instructions, searching existing data sources, gathering and maintaining the data needed, and completing and reviewing the collection of information. Send comments regarding this burden estimate or any other aspect of this collection of information, including suggestions for reducing this burden, to Washington Headquarters Services, Directorate for Information Operations and Reports, 1215 Jefferson Davis Highway, Suite 1204, Arlington, VA 22202-4302, and to the Office of Management and Budget, Paperwork Reduction Project (0704-0188), Washington, DC 20503.

1. AGENCY USE ONLY *(Leave blank)*	2. REPORT DATE **July 1992**	3. REPORT TYPE AND DATES COVERED Final, January 1989–January 1991

4. TITLE AND SUBTITLE

Numerical Experiments on Adiabatic Shear
Band Formation in One Dimension

5. FUNDING NUMBERS

PR: 1L161102AH43

6. AUTHOR(S)

John W. Walter, Jr.

7. PERFORMING ORGANIZATION NAME(S) AND ADDRESS(ES)

8. PERFORMING ORGANIZATION REPORT NUMBER

9. SPONSORING / MONITORING AGENCY NAME(S) AND ADDRESS(ES)

U.S. Army Ballistic Research Laboratory
ATTN: SLCBR-DD-T
Aberdeen Proving Ground, MD 21005-5066

10. SPONSORING / MONITORING AGENCY REPORT NUMBER

BRL-TR-3381

11. SUPPLEMENTARY NOTES
Paper has been reviewed by and accepted for publication in the International Journal of Plasticity.

12a. DISTRIBUTION / AVAILABILITY STATEMENT
Approved for public release; distribution is unlimited.

12b. DISTRIBUTION CODE

13. ABSTRACT *(Maximum 200 words)*

Adiabatic shear band formation in an elastic, thermo-visco-plastic, simple material is studied in the context of unidirectional shearing of a slab. The effect of varying the thermal softening behavior of the material on localization strain and post-localization morphology is studied for a rigid, perfectly plastic material; the material parameters are appropriate for a high-strength steel. In this case, it is demonstrated that localization of the strain rate can be *transient*. A coupling between linear-elastic response and the basic thermo-visco-plastic localization mechanism is explored in the absence of strain hardening. Lastly, the flow law is modified to include strain hardening in order to simulate a high-rate torsion test on OFHC copper. In this case, localization is initiated by thermal boundary layer diffusion, and the solution takes on a complex, apparently nonperiodic, post-localization morphology quite different from that in the perfectly-plastic cases.

14. SUBJECT TERMS

plastic properties, finite element analysis, elastic waves, thermomechanics

15. NUMBER OF PAGES
83

16. PRICE CODE

17. SECURITY CLASSIFICATION OF REPORT	18. SECURITY CLASSIFICATION OF THIS PAGE	19. SECURITY CLASSIFICATION OF ABSTRACT	20. LIMITATION OF ABSTRACT
UNCLASSIFIED	UNCLASSIFIED	UNCLASSIFIED	SAR

INTENTIONALLY LEFT BLANK.

TABLE OF CONTENTS

DTIC QUALITY INSPECTED 2

INTENTIONALLY LEFT BLANK.

LIST OF FIGURES

ACKNOWLEDGEMENT

INTENTIONALLY LEFT BLANK.

1. INTRODUCTION

The phenomenon of adiabatic shear localization has received increasing attention in recent years as it is a primary mode of ductile deformation and failure in a variety of materials at moderate-to-high rates of deformation. Indeed, it has long been known to be crucial in situations such as machining, metal forming, shock loading, and ballistic impact and penetration, and has even been proposed as an explanation for deep earthquakes (Frohlich 1989). The basic mechanism for adiabatic localization is an *autocatalytic* process of local heating (due to plastic work) accompanied by thermal softening which, if strong enough to overcome strain and strain rate hardening, causes an increase in the local rate of plastic work and, in turn, intensifies the heating. Of course, plastic flow localization may also occur by other softening mechanisms such as texture development at large strains or ductile void growth; these mechanisms may act in concert with thermal softening in the formation of physical shear bands but this paper focuses strictly on the latter. While recognition of thermal softening as a localization mechanism dates back to Tresca (1878) (see the article by Johnson [1987]) and more recently to Zener and Hollomon (1944), it is only during the last 10–15 years that there has been a fairly steady effort to analyze and model this phenomenon. Consequently, even the qualitative behavior of rather simple material models remains largely unexplored in this context.

The purpose of this article is to document some recent numerical experiments and analytical results which extend those of Wright and Walter (1987). As in that investigation, we consider a simple model problem for shear localization (namely the unidirectional simple shear of an infinite slab) which simulates some aspects of experiments such as the "pressure-shear" test (Clifton 1990) and the thin-wall tube torsion test (Hartley et al. 1987; Lindholm et al. 1980). It should be noted that this model problem ignores a number of potentially important aspects of both of these types of experiments. For example, while the pressure-shear experiment is generally felt to be one-dimensional (until lateral unloading waves impinge upon the sample), it is *not* unidirectional and a more complete simulation would account for the pressure-volume response of the material and effects of pressure or volume change on the material's distortional response. In the case of the thin-wall tube test, the material in the specimen gauge length is more nearly in a state of plane-stress than of plane-strain as our model problem assumes. Moreover, the work of Duffy and co-workers (Hartley et al. 1987;

1

Marchand and Duffy 1988) has illustrated clearly that the process of shear band formation in such a test is generally *not* axially symmetric. However, in spite of its simplicity, the problem formulation given in Section 2 incorporates the essential material behaviors necessary for shear band modeling as noted in Wright and Walter (1987): local heating by plastic working, local heat conduction, thermal softening, and strain rate hardening.

The simplified material model just described is referred to in the sequel as a rigid, perfectly plastic (RPP) material and the specific instance of this material used previously (*ibid*) is considered a "baseline" case against which to compare results for the more complex material models used here. The homogeneous solution and the linearized perturbation solution obtained previously for a RPP material (*ibid*) are extended in Section 3 to account for a time-dependent boundary velocity. In addition, analytic inequalities are obtained which describe the effect of varying the thermal softening behavior of the flow law on the perturbation solution. In Section 4.1, variation of the thermal softening behavior is considered numerically* for a thermally insulated initial-boundary-value-problem (IBVP) with material parameters characteristic of a high-strength steel as were used previously (*ibid*). These results are used to evaluate the validity of several analytical "localization" criteria which have appeared in the literature. Because the thermal softening behavior of the flow law enters into different localization criteria in very different ways, the softening variants employed were selected *specifically* to emphasize these differences when compared with the numerical results; ability to fit any specific material data was *not* the primary concern. In Section 4.2, the same IBVP is considered; but for an elastic, perfectly plastic material. An interesting coupling between the linear elastic response and the basic thermo-visco-plastic localization mechanism is explored there. Section 4.3 concerns the simulation of a moderately high rate, thin-wall tube, torsion test on OFHC copper using an IBVP with temperature held fixed at the outside of the slab. Results from this problem show how shear band formation may initiate through boundary layer diffusion in the absence of an introduced perturbation. They also illustrate that strain hardening can produce solutions with complex, seemingly nonperiodic morphologies and show the strong dependence of localization length scales on the material parameters.

---

*Some details concerning the numerical method employed appear in the Appendix.

2. PROBLEM FORMULATION

The model problem considered is the unidirectional shearing of a slab of an incompressible material which occupies the region between the planes $Y = \pm h$. The field equations and nondimensionalization used are essentially those of Wright and Batra (1985) and Wright and Walter (1987); we outline their derivation here for completeness. We suppose the motion is volume preserving and, with X as the direction of shear, may be written as

$$x = X + u(Y,t), \quad y = Y, \quad z = Z, \tag{1}$$

where (x,y,z) is the position at time t of the material particle whose reference position (at time $t = 0$) was (X,Y,Z). The dimensional equations expressing balance of momentum, energy, and entropy in the absence of body forces and external heat supply take the form

$$s_y - \rho \dot{\upsilon} = 0,$$
$$\rho \dot{U} + q_y - s\eta_y = 0,$$
$$\rho T\dot{\eta} - (q/T)T_y + \dot{q}_y \geq 0, \tag{2}$$

where $\upsilon = \dot{u}$ is the velocity in the $y\, (= Y)$ direction, s is the single nonzero component of the Cauchy stress tensor, U is the internal energy per unit mass, q is the y-component of the heat flux, T is the absolute temperature, η is the entropy per unit mass, and ρ the (constant) mass density. We will use the superposed dot and subscript y to indicate differentiation with respect to time t and the spatial variable y, respectively. We also assume that the total shear strain γ can be decomposed additively into elastic and plastic parts

$$\gamma = u_y = \gamma_e + \gamma_p, \tag{3}$$

which implies a corresponding decomposition for the velocity gradient.

Since plastic flow limits the magnitude of the shear stress, we need consider only linear elastic response, and we also restrict attention to linear heat conduction with no thermoelastic effects or phase transitions. With regard to the plastic response, we assume that the stress in a slow, monotone, isothermal shearing at the ambient temperature T_o is described by $s = \kappa(\psi)$, where ψ is the plastic strain in that case. We also assume that strain hardening evolves according to the total plastic work done, regardless of rate, so that

3

$$\dot{W}_p = \kappa(\psi)\dot{\psi} = s\dot{\gamma}_p, \tag{4}$$

which describes the evolution of the strain hardening variable ψ; here $\dot{\gamma}_p$ is the single nonzero component of the plastic strain rate tensor, not a von Mises equivalent rate. It should be emphasized that shearing of the sort considered here would typically produce normal stresses in the y direction and an accompanying pressure which could be expected to influence the plastic response of the material. The large deformations and temperature changes which are known to occur in adiabatic shear bands (Hartley et al. 1987) might also induce phase changes. However, we ignore all such effects here. With these assumptions, we may write the field equations as

$$p\dot{v} = s_y,$$
$$\rho c_v \dot{\theta} = k\theta_{yy} + s\dot{\gamma}_p,$$
$$\dot{s} = \mu(v_y - \dot{\gamma}_p),$$
$$\dot{\psi} = s\dot{\gamma}_p/\kappa(\psi), \tag{5}$$

in which $\theta = T - T_o$ is the temperature relative to ambient, μ is the shear modulus, c_v is the specific heat at constant volume, and k is the thermal conductivity. We will consider a rate dependent flow law of the general form

$$s = G(\theta,\psi,\dot{\gamma}_p), \tag{6}$$

where, for simplicity, we assume that $\dot{\gamma}_p$ is real and θ and ψ are non-negative. Moreover, we require that G satisfy the conditions

$$\frac{\partial G}{\partial \lambda}(\lambda\theta,\psi,\dot{\gamma}_p) < 0, \quad \frac{\partial G}{\partial \lambda}(\theta,\lambda\psi,\dot{\gamma}_p) > 0, \quad \frac{\partial G}{\partial \lambda}(\theta,\psi,\lambda\dot{\gamma}_p) > 0, \tag{7}$$

for all positive λ and for all $(\theta,\psi,\dot{\gamma}_p)$ in the domain of G with $\dot{\gamma}_p \neq 0$, so that the flow law exhibits thermal softening, strain hardening, and strain rate hardening. The flow law may or may not possess a non-null elastic range; but if it does, then the yield surface is described by

$$|s| - G(\theta,\psi,0) = 0, \tag{8}$$

with the criteria for elastic or plastic behavior being given respectively by

$$|s| \leq G(\theta,\psi,0), \quad |s| > G(\theta,\psi,0). \tag{9}$$

4

Because the stress s appears in Equations (8) and (9) only through its absolute value, the model cannot account for asymmetric unloading response such as the Bauschinger effect. In view of Equation $(7)_3$, we may invert the flow law to obtain

$$\dot{\gamma}_p = H(\theta, \psi, s),\qquad (10)$$

and it is this form which will prove most useful for computations.

Specifically, we shall employ several variants of a multiplicative overstress type of flow law similar to that introduced by Litoński (1977)

$$G(\theta, \psi, \dot{\gamma}_p) = \kappa(\psi) g(\theta) f(\dot{\gamma}_p).\qquad (11)$$

The thermal softening factor variants to be considered are

$$g_1 = (1 - a\theta/0.9)^{0.9}, \quad g_2 = 1 - a\theta, \quad g_3 = e^{-a\theta}, \quad g_4 = \frac{1}{2}(1 + e^{-a\theta}),\qquad (12)$$

and we will use them in combination with the strain hardening factor

$$\kappa = \kappa_o\left(1 + (\psi/\psi_o)^n\right),\qquad (13)$$

and the strain rate hardening factor variants

$$f_1 = \operatorname{sgn}(\dot{\gamma}_p)(1 + b|\dot{\gamma}_p|)^m, \quad f_2 = \operatorname{sgn}(\dot{\gamma}_p)\left(1 + m\ln(b|\dot{\gamma}_p|)\right).\qquad (14)$$

Here $a, \kappa_o, \psi_o, n, b, m$ are constant material parameters and sgn indicates the algebraic sign of its argument. Note that Equations (13) and $(14)_2$ are the forms used by Johnson and Cook (1983); motivation for this selection of thermal softening factors is given in Section 4.1.

The nondimensional forms of the governing equations result by replacing Equations (5) and (13) with

$$\dot{v} = s_y/\rho,$$
$$\dot{\theta} = \kappa\theta_{yy} + s\dot{\gamma}_p,$$
$$\dot{s} = \mu\left(v_y - \dot{\gamma}_p\right),$$
$$\dot{\psi} = s\dot{\gamma}_p/\kappa(\psi),\qquad (15)$$

and

5

$$\kappa_1(\psi) = (1 + \psi/\psi_o)^n, \quad \kappa_2(\psi) = \left(1 + (\psi/\psi_o)^n\right), \tag{16}$$

respectively, while Equations (12) and (14) are unchanged. The complete set of nondimensional parameters and variables appearing in Equations (12) and (14)–(16) and the relations to their dimensional counterparts (barred here to distinguish them) are

$$\rho = \bar{\rho}\bar{h}^2 \dot{\bar{\gamma}}_o^2/\bar{\kappa}_o, \quad k = \bar{k}/\bar{\rho}\bar{c}_v\bar{h}^2 \dot{\bar{\gamma}}_o,$$

$$\mu = \bar{\mu}/\bar{\kappa}_o, \quad b = \bar{b}\dot{\bar{\gamma}}_o, \quad a = \bar{a}\bar{\kappa}_o/\bar{\rho}\bar{c}_v, \tag{17}$$

and

$$y = \bar{y}/\bar{h}, \quad t = \bar{t}\dot{\bar{\gamma}}_0, \quad \upsilon = \bar{\upsilon}/\bar{h}\dot{\bar{\gamma}}_o, \quad s = \bar{s}/\bar{\kappa}_o,$$

$$\theta = \bar{\theta}\bar{\rho}\bar{c}_v/\bar{\kappa}_o, \quad \kappa = \bar{\kappa}/\bar{\kappa}_o, \quad \dot{\gamma}_p = \dot{\bar{\gamma}}_p/\dot{\bar{\gamma}}_o, \tag{18}$$

in which $\bar{h}$ is one-half the thickness of the slab, $\dot{\bar{\gamma}}_o = \bar{V}_o/\bar{h}$ is the characteristic nominal strain rate, $\bar{V}_o$ is a characteristic value of the velocity imposed at the boundary, and $\bar{\kappa}_o$ is the initial yield strength of the material. Throughout the sequel, we suppose that the problem is symmetric about the slab center so that

$$\upsilon(0,t) = 0, \quad \theta_y(0,t) = 0. \tag{19}$$

The conditions imposed at the specimen boundary by a loading device in an experiment are generally complex, and we do not attempt to model them in any detail here. Instead, we shall examine the limiting cases with respect to the thermal boundary condition. First, in order to compare directly with Wright and Walter (1987) and Wright (1990b), we assume in Sections 4.1 and 4.2 a constant velocity and *thermally insulated* outer boundary for which

$$\upsilon(1,t) = 1, \quad \theta_y(1,t) = 0, \tag{20}$$

and, in Section 4.3, we assume a constant velocity and *perfectly conducting* outer boundary for which

$$\upsilon(1,t) = 1, \quad \theta(1,t) = 0. \tag{21}$$

6

Because the boundary velocity is constant, Equation (18) implies that

$$\gamma_o = \dot{\bar{\gamma}}_o \bar{t} = t,\tag{22}$$

where γ_o is the nominal strain (boundary displacement divided by thickness). Initial conditions to complete specification of the IBVP will be given as each problem is considered.

3. PERTURBATION ANALYSIS FOR A RIGID, PERFECTLY PLASTIC MATERIAL

Wright (1990b) and Wright and Walter (1987) have performed linearized perturbation analyses for several specializations of the problem class described in Section 2, but in all cases for a constant velocity imposed at the outer boundary. Here we present similar results which account for an arbitrary time-dependence of the imposed velocity and analyze the effect on the perturbation solution of the different thermal softening variants. These results are used to elucidate some of the numerical results reported in Section 4.1.

We restrict attention to a *quasi-static* specialization of the thermally insulated problem (Equation 20) for the RPP material model. In the quasi-static specialization (which was shown to be valid up to moderate strain rates for the problem considered *ibid*), the stress is independent of y and the momentum equation (Equation [15]$_1$) is dropped. In addition, the evolution equation (Equation [15]$_4$) for ψ is dropped, the strain hardening factor κ is replaced by unity in the flow law (Equation [11]), and $\dot{\gamma}_p$ is replaced by υ_y in the energy equation (Equation [15]$_2$). The stress is now determined by the flow law, $s = G(\theta, 0, \upsilon_y)$, rather than by the rate equation (Equation [15]$_3$). To incorporate the variable boundary velocity into the field equations, we replace definition (Equation [18]) of the nondimensional velocity $\upsilon = \bar{\upsilon}/\bar{V}_o$ with

$$\upsilon = \frac{1}{v(t)} \frac{\bar{\upsilon}}{\bar{V}_o} = \frac{\bar{\upsilon}}{\bar{V}(t)}.\tag{23}$$

in which $v(t) = \bar{V}(t)/\bar{V}_o$ is the nondimensional velocity imposed at the boundary, $\bar{V}(t)$ is its dimensional counterpart, and $\bar{V}_o$ is a characteristic value of $\bar{V}(t)$. Thus, instead of scaling $\bar{\upsilon}$

by the constant value $\bar{V}_o$, here we scale by the time-dependent value $\bar{V}(t)$. With these assumptions, the quasi-static field equations reduce to

$$\dot{\theta} = k\theta_{yy} + sv\upsilon_y , \quad s = g(\theta)f(v\upsilon_y) , \tag{24}$$

where f and g are as in Equation (11), the boundary conditions are as in Equations (19) and (20). With spatially homogeneous initial conditions

$$\upsilon_y(y,0) = 1 , \quad \theta(y,0) = \theta_I , \quad s(0) = g(\theta_I) f\big(v(0)\big) , \tag{25}$$

there is a homogeneous solution of the form

$$\upsilon_{H_y}(t) = 1 , \quad s_H(t) = g(\theta_H(t))f\big(v(t)\big) , \tag{26}$$

where $\theta_H(t)$ is determined by

$$\int_{\theta_I}^{\theta_H(t)} \frac{d\theta}{g(\theta)} = \int_o^t f\big(v(t')\big)v(t')dt' . \tag{27}$$

If $\bar{V}(t)$ is constant and the boundary conditions are as assumed here, then the original field Equations (15) also have a homogeneous solution. However, if $\bar{V}(t)$ is *not* constant, then a homogeneous solution exists *only* in the context of the quasi-static specialization.

Next, we obtain a closed-form linear perturbation solution to Equation (24) and the accompanying absolute stability criterion.* We assume an expansion of the form

$$\theta = \theta_H(t) + \bar{\theta}(y,t) , \quad s = s_H(t) , \quad \upsilon = \upsilon_H(t) + \bar{\upsilon}(y,t) , \tag{28}$$

in which the *mean value* of the temperature perturbation has been absorbed into θ_H (which also ensures that the stress perturbation vanishes identically) and θ is the temperature

---

*A perturbation analysis of this sort, which includes exactly the time variation of the homogeneous solution, was first given by Wright and Walter (1987) for a constant boundary velocity and the particular flow law given by Equations (12)₂ and (14)₁. Further analyses, which include (for *constant* boundary velocity) combined effects of thermal softening, strain and strain rate hardening, and heat conduction, have been presented by Wright (1990a, 1992).

perturbation *about mean.*[*] On substituting these expressions into Equation (24), expanding, retaining only terms of first order in the perturbations, and rearranging there follows

$$\bar{v}_y = - \frac{g'_H f_H \bar{\theta}}{gH f'_H v} , \quad \bar{\theta}_t = k\bar{\theta}_{yy} - \frac{g'_H f_H^2}{f'_H}\bar{\theta} , \tag{29}$$

with boundary conditions

$$\bar{\theta}_y = \bar{v} = 0 \text{ at } y = 0 \text{ and } y = 1 . \tag{30}$$

This problem admits a solution in the form

$$\bar{\theta}(y,t) = \sum_{n=1}^{\infty} \phi_n \cos(n\pi y) \exp\left(- \int_o^t [w(r) + k(n\pi)^2]dr \right) ,$$

$$\phi_n = 2 \int_o^1 (\theta_I(y) - \theta_H(0))\cos(n\pi y) dy , \tag{31}$$

where $w = g'_H f_H^2 / f'_H$, $\theta_H(0) = \int_o^1 \theta_I dy$ and $\bar{v}$ is recovered from Equation (29). The condition for absolute stability follows by noting that since $w(t) < 0$ at all times, the first Fourier component of $\bar{\theta}$ has the algebraically largest time rate. Thus, the homogeneous solution is infinitesimally stable provided

$$- \frac{g'_H f_H^2}{f'_H} < k\pi^2 . \tag{32}$$

This result shows that the homogeneous solution may lose or regain stability as $\bar{V}$ varies and that current stability depends only on the current value of $\bar{V}$ and *not* on its history.

To ascertain the dependence upon the thermal softening variant of the linear perturbation solution and stability condition, we need inequalities relating the coefficient functions $g_H(t)$ and $g'_H(t)$ for the thermal softening factor variants in Equation (12). First, consider two

---

[*]This simplification was suggested by T. Wright.

variants with one *softer* than the other in the sense that $g_1(\theta) \le g_2(\theta)$ for all θ in their common domain. Then Equation (27) implies the inequality

$$\theta_{1H}(t) \le \theta_{2H}(t), \text{ for } t > 0 . \tag{33}$$

However, as the softening variants are monotone decreasing, this inequality does *not* imply any definite relationship between $g_{1H}(t)$ and $g_{2H}(t)$. Since general results are not apparent, we instead consider the specific variants in Equation (12). We will refer to them as enumerated there, except for g_1 which is a member of the α-parameterized family

$$g_\alpha(\theta) = (1 - a\theta/\alpha)^\alpha, \text{ for } 0 < \alpha < 1, 0 \le \theta \le \alpha/a . \tag{34}$$

As is easily verified, these functions each satisfy the conditions

$$g(0) = 1, g'(0) = -a , \tag{35}$$

and the inequalities

$$g_\alpha''(\theta) < g_2''(\theta) = 0 < g_3''(\theta) < g_4''(\theta), \text{ for } 0 < \alpha < 1 , \tag{36}$$

over their common domains. The family g_α also satisfies the inequality

$$g_{\alpha_1}''(\theta) < g_{\alpha_2}''(\theta), \text{ for } 0 < \alpha_1 < \alpha_2 < 1 . \tag{37}$$

Note that Equations (35)–(37) imply analogous inequalities for the first derivatives and function values, and it is convenient to consider the g's as *ordered* by Equations (36) and (37). With this ordering of the softening variants, it is not difficult to show, for 0 , $\alpha_1 < \alpha_2 < 1$ and all t in the domain of the respective θ_H, that the perturbation coefficient functions follow the same order

$$0 < g_{\alpha_1 H}(t) < g_{\alpha_2 H}(t) < g_{2H}(t) < g_{3H}(t) < g_{4H}(t) ,$$

$$g'_{\alpha_1 H}(t) < g'_{\alpha_2 H}(t) < g'_{2H}(t) < g'_{3H}(t) < g'_{4H}(t) < 0 . \tag{38}$$

Thus, the perturbation solution shows that, other things being the same, more rapid thermal softening implies *smaller* magnitudes for θ_H and $s = s_H$, but *larger* magnitudes for $\hat{\theta}$ and $\hat{v}_y$.

10

As might be expected, more rapid softening is *destabilizing* in the sense that a softer g yields, at each time t, an algebraically larger value on the left side of Equation (32).

4. NUMERICAL RESULTS

In this section, we consider the effect of several variants of the material model on the pre-and post-localization behavior of the shear band problems posed in Section 2. In Sections 4.1 and 4.2, we assume the boundary conditions at $y = 1$ are as in Equation (20) so that the IBVP possesses a homogeneous solution as outlined in Section 3. There are many sets of initial conditions (i.e., perturbations) which can evolve into a single band at the slab center, but we consider only one possibility. Moreover, we are not concerned here with early transient response and, in view of Equations (15)$_1$ and (15)$_3$, the *initial* time rates of velocity and stress may be made to vanish by imposing initial conditions of the form

$$s(y,0) = s_I = \text{const}, \ \upsilon_y(y,0) = \dot{\gamma}_p(y,0), \ \psi(y,0) = \psi_I = \text{const}, \tag{39}$$

where subscript I indicates an initial value. The initial velocity gradient follows from the flow law (Equation [10]) as

$$\upsilon_{yI}(y) = \dot{\gamma}_{pI}(y) = H(\theta_I(y), \psi_I, s_I) . \tag{40}$$

To afford comparison with previous results of Wright and Walter (1987), we use the same temperature perturbation as used there and assume no initial plastic deformation

$$\theta_I(y) = 0.1(1 - y^2)^9 e^{-5y^2}, \ \psi_I = 0 . \tag{41}$$

To avoid a singularity, Equation (40) must be consistent with the boundary condition (Equation [20]$_1$) and this is achieved simply by using an appropriate value of s_I. Lastly, in Sections 4.1 and 4.2, we assume material parameters as in Table 1 and slab thickness $h = 3.47$ mm as used before (*ibid*).

4.1. Effect of Thermal Softening Variation. Here we examine effects due to qualitatively varying the thermal softening behavior (Equation [12]) of the flow law independently of strain hardening or elasticity. Computationally, these effects are nullified by setting the strain hardening parameter n to zero and using a value of the shear modulus much larger (e.g.,

Table 1. Material Parameter Values in SI Units for a Moderately High-Strength Steel

$\bar{\rho}$	$\bar{k}$	$\bar{c}_\upsilon$	$\bar{a}$	$\bar{b}$
7860	49.2	473	6.43×10^{-4}	10^4
m	$\bar{\mu}$	ψ_o	n	$\bar{\kappa}_o$
0.0251	8×10^{10}	0.017	0.09	6.02×10^8

1,000 times) than that given in Table 1. Because the shear stress is limited by the flow law, the increased modulus ensures that the stored elastic energy is reduced to an insignificant level. The four softening variants have very different behavior for large θ, but are normalized in the sense that (for the same value of a, chosen as $1/\theta_{melt}$ where θ_{melt} is the dimensionless melting temperature) they have the same value and slope at $\theta = 0$

$$g_1(\theta) \rightarrow) \text{ as } \theta \rightarrow 0.9/a$$

$$g_2(\theta) \rightarrow 0 \text{ as } \theta \rightarrow 1/a$$

$$g_3(\theta) \rightarrow 0 \text{ as } \theta \rightarrow \infty$$

$$g_4(\theta) \rightarrow 0.5 \text{ as } \theta \rightarrow \infty .$$ (42)

The linear variant g_2 is known to be exceptional, in that it admits a "quasi-steady" post-localization solution (ibid) in which the velocity gradually becomes time-independent following localization. It is also the "boundary case" ($g'' = 0$) between classes of softening variants which are strictly concave ($g'' < 0$) and strictly convex ($g'' > 0$). Hence, we examine variant g_1 as an example of the former class and g_3 for the latter. Variant g_4 is considered because, in contrast with the other three variants, it tends to a positive value for large θ. Strain rate factor (Equation [14]$_1$) is used here and in Section 4.2.

As a baseline result, we consider the same linear thermally softening case ($g(\theta) = g_2(\theta)$ and $\dot{\bar{\gamma}}_o = 500/s$) as reported by Wright and Walter (1987). The plastic strain rate $\dot{\gamma}_p$ (in this subsection numerically equal to υ_y) is plotted as a function of the spatial coordinate y and nominal strain γ_o in Figure 1. Regarding these solution surface plots, we note that the logarithmic y-axis scale is often necessary to resolve highly localized band structures and it is

12

sometimes necessary to reorient the base-plane axes on the plot in order to display certain portions of the surface. Also, since the nominal strain and dimensionless time are numerically equal in this section (Equation [22]), we will use the symbol γ_o as the time-axis label and use it sometimes when referring to the time t. Figure 1 clearly shows the three-stage band formation process of slow early growth, then sudden localization after a delay, followed by slow post-localization variation. Referring to Figure 2 (note the expanded time axis), the temperature is fairly low compared to $\theta_{melt} \approx 10$ and the stress close to its homogeneous value until just before localization while the maximum time rates of $\dot{\gamma}_p$, θ, and s occur simultaneously. Note also that the internal time step ΔT_s used by the differential equation integrator is much reduced during the rapid localization, indicating numerical stiffness in the system of equations (Equation [A-10]), and then returns to an imposed maximum value. These results agree exactly with those reported previously (ibid) which serves as a check on the finite element method used here and on the efficacy of the artificial elastic modulus approximation to the RPP material model.

A consequence of the weak strain rate hardening ($m << 1$) is that $\dot{\gamma}_p$ undergoes very large deviations during localization from its values in the homogeneous solution. Thus, the differences between the softening variants may be seen most easily in plots of this variable, which appear as Figures 3, 4, and 5. As shown previously (ibid), the asymptotically steady behavior of $\dot{\gamma}_p$ holds only for linear thermal softening. The severity of localization is emphasized by referring to Equation (18), whence the maximum dimensional strain rates at the slab center for $\gamma_o \leq 1$ range from 2.1×10^5/s for softening variant g_4 to 10^6/s for softening variant g_1. Note that for the concave variant g_1, the strain rate localization intensifies during the third stage but, for the convex variants g_3, and especially g_4, the strain rate localization decays during the third stage.

A crucial aspect of the band formation process is the delay between loss of stability of the underlying homogeneous solution and the occurrence of severe localization with its attendant stress collapse. As may be seen in Figure 1, this delay is substantial even though the homogeneous solution is unstable at all times in this case. As previously (ibid), the localization strain γ_{loc} is defined as the value of γ_o at which $d\dot{\gamma}_p(0,\gamma_p)/d\gamma_o$ attains its

maximum. The values of $\dot{\gamma}_p$, θ, and s at the slab center are plotted in Figures 6–8 against γ_o and γ_{loc}, is summarized in Table 2. Note that the values of γ_{loc} order in the same way as the softening functions were ordered in Section 3. This ordering is also apparent in the pre- and post-localization levels of strain rate and stress, with the central values of both fields sustaining the largest deviation from homogeneous response for the softest variant, g_1. The behavior of the temperature is more complicated. Before localization (e.g., $\gamma_o = 0.24$) the central values are ordered in opposition to inequality (Equation [36]) but, referring to Figure 7, the post-localization order is reversed so that variant g_4 sustains the largest temperatures during the late stage.

Table 2. Variation of Nominal Strain, γ_o at Localization With Thermal Softening Variant for Initial Conditions (Equations [39]–[41]) at $\dot{\gamma}_o = 500/s$ as Computed by the Finite Element Method and by the Locally Adiabatic Solution of Wright Described in Section 4.1

Softening Variant	g_1	g_2	g_3	g_4
$(\gamma_{loc})_{fem}$	0.262	0.265	0.285	0.320
$(\gamma_{loc})_{Wright}$	0.252	0.254	0.273	0.298

The linear perturbation analysis in Section 3 provides qualitative agreement with the numerically observed effect of the different softening variants as follows. The initial values of $\theta_H(0), \theta_{Ht}(0), \bar{\theta}(0,0), \bar{\theta}_t(0,0)$, are respectively equal to 0.023, 1.47, 0.077, 6.11. Note that the central value of $\bar{\theta}$ is initially both larger and increasing more rapidly than is θ_H. Even at a time after the perturbation solution has lost validity (e.g., when $\theta_H \approx 1$), θ_{Ht} ranges from 1.31 (for g_1) to 1.33 (for g_4) while $\bar{\theta}_t$ still has larger values ranging from 6.17 to 4.96. Thus, although $\theta_H(t)$ increases less rapidly for a softer g-function, $\bar{\theta}(0,t)$ more than compensates producing larger central temperatures. As noted at the end of Section 3., a softer g also yields larger υ_y and smaller s, all of which agree with the numerical results.

This reversal in the ordering of the central temperatures during severe localization is counter intuitive since the central values of accumulated plastic work continue in the same order as did the central values of θ prior to localization. Figure 9 shows the accumulated plastic work as a function of y (note the log axis) at $\gamma_o = 0.5$ which is well into the post-localization stage. Observe, however, that the width of the band* w_{sb} just after severe localization is smaller by about a factor of 10 for variant g_1 as compared to g_4. While the intensity of plastic working (and, consequently, of heat production) at the band center is much larger for variant g_1, so also is the effect of heat conduction because the band is narrower. Indeed, the effect of the dimensionless thermal length scale $l_\theta = k^{1/2} = 0.046$ may clearly be seen by comparing the post-localization profiles of plastic work in Figure 9 with the temperature profiles in Figure 10; note the logarithmic y-axis scale in each case. When $l_\theta >> w_{sb}$, as is the case here for all the softening variants and particularly g_1 and g_2, the near-center θ profile very quickly becomes independent of the profile of $\dot{\gamma}_p$. Immediately following rapid localization, the θ profile is essentially determined by the total rate of work supplied through the outer boundary and the thermal diffusion which would occur if this energy were supplied as a heat flux through the boundary at $y = 0$. The opposite, approximately adiabatic case with $l_\theta << w_{sb}$ (which characterizes the prelocalization regime for the diffuse perturbation [Equation (41),] used here) would persist only if the localization were much weaker. In such a case, $\dot{W}_p$ would be nontrivial at lengths *greater* that w_{sb} and the θ profile would be primarily determined by the local value of $\dot{W}_p$ rather than by thermal diffusion.

Next, we turn to evaluation of several *analytical* criteria for shear band formation which have appeared in the literature. Because some of these criteria depend on the long time ($t \rightarrow \infty$) behavior of analytical solutions to shear band problems, it is necessary to consider this limit numerically as well.** As noted above, the choice of softening variant has

---

* In rough terms W_{sb} is the width of the material layer which is being plastically worked at a nontrivial rate. For the problem considered here, we define W_{sb} to be twice the value of y at which $\dot{W}_p$ (or $\dot{\gamma}_p$, since s is uniform) drops to 10% of its value at $y = 0$; compare the solution surfaces for $\dot{\gamma}_p$ with Figure 9.

**Both analysis and numerics at long times may be criticized as "lacking physicality." However, it is sometimes the case that such results *do* bear on what occurs at earlier times. It is this question that we explore here.

substantial effect on the post-localization profile of $\dot{\gamma}_p$. Referring to Figure 11, by the time γ_o = 20 the central value of $\dot{\gamma}_p$ has decayed from its peak to a value of about 150 for variant g_3, but to a value of about 3 for variant g_4. For the latter, it appears that $v_y(y,t) \to 1$ as $t \to \infty$, which also implies that $\gamma(y,t)$ is asymptotic to $\gamma_o = t$ in the same limit. Since the stress remains independent of y, this implies that $\dot{W}_p(y,t) \to 1/2$ in view of Equation (42)$_4$. In view of the thermally insulated boundary at $y = 1$ and asymptotically y-independent heat production, the mean temperature will continue to increase without bound but with $(\theta_{max} - \theta_{min}) \to 0$. Thus, while the other softening variants yield persistent localization of $\dot{\gamma}_p$, variant g_4 appears to lead to a state of *uniform shearing* as $t \to \infty$.

In this connection, Tzavaras (1986) has considered the locally adiabatic version ($k = 0$) of the current problem for a RPP material with flow law

$$s = g(\theta)\mathrm{sgn}(v_y)|v_y|^m, \quad g(\theta) > 0, \quad g'(\theta) < 0, \quad \theta \varepsilon (0,\infty). \qquad (43)$$

Assuming sufficient smoothness of the initial data, he concludes that if there exists some $v < 0$ and $N < \infty$ such that

$$1 + \frac{1}{m} < 1 - \frac{1}{v} \le \frac{g(\theta)g''(\theta)}{g'(\theta)^2} \le N, \qquad \text{for all } \theta \varepsilon (0,\infty), \qquad (44)$$

then every classical solution (to the momentum and energy balance equations) tends to a state of uniform shearing as $t \to \infty$. Note that this conclusion still follows if Equation (44) holds only for all θ larger than some fixed value. It is interesting to note that Equation (44) cannot be satisfied for the first three softening variants for any θ in their respective domains and, as the finite element calculations indicate, localization of $\dot{\gamma}_p$ is persistent in these cases. However, for variant g_4, Equation (44) *is* satisfied provided $\theta > 17.7$, so that after an initial localization, Tzavaras' theorem predicts eventual uniform shearing in qualitative agreement with our numerical results.[*] Hence, while his theorem is correct as stated, it does *not*

---

[*]Since Tzavaras assumed $\rho = c_v = 1$, the values of his dimensionless parameters are different from those used here and quantitative comparison is not possible. Also, since heat conduction is stabilizing, strain rate decay begins at lower temperatures in the numerical calculation (when $\theta(0,t) \approx 5$) than would be expected from Tzavaras' locally adiabatic analysis, as may be seen by comparing Figures 6 and 7.

preclude localization unless Equation (44) is satisfied for *all* $\theta \ \epsilon \ (\theta_{min}, \infty)$, where

$\theta_{mi-} = \min_{0<y<1} \theta_i(y)$.

Another example is the paper of Molinari and Clifton (1987) in which the simple shear problem is viewed as an approximation to the torsion of a thin walled tube at high strain rate. Using a locally adiabatic, quasi-static analysis for a material with flow law of the form Equation (43), the same boundary conditions as used here, and a perturbation in either the wall thickness or initial temperature, they obtain a criterion for "L_--localization" (by which is meant the $\theta(y_L, t) \rightarrow \infty$ as $t \rightarrow \infty$) at the position y_L for which

$$\ell(y_L)^{(1+m)/m} \int_{\theta_I(y_L)}^{\infty} g(\theta)^{1/m} \, d\theta < \infty , \tag{45}$$

attains its minimum value with respect to y. Here ℓ is the tube wall thickness and θ_I is the initial temperature. Of course, this result depends on convergence of the integral in Equation (45) at each y and nonconvergence (the case for softening variant g_4) implies that L_--localization does not occur. Hence, because of its emphasis on the high-temperature behavior of the flow law, this criterion correctly detects the trend toward uniform shearing at long time, but fails to catch the earlier transient localization.

In contrast with these examples, Wright (1990b) has obtained an approximate "parametric" solution for the quasi-static, perfectly plastic problem. In general, this scheme involves solution of the heat equation with a nonlinear source term, followed by a pair of numerical quadratures. The calculations required to obtain γ_{loc} may be performed easily on a personal computer. The values of γ_{loc} so obtained agree closely with those from finite element computations over a wide range of the nominal strain rate (Wright 1990b, Figure 2). For the quasi-static, locally adiabatic problem (with or without strain hardening), Wright's scheme provides an exact solution and for the RPP material it requires only two numerical quadratures. The latter form was computer-coded independently and, as Table 2 illustrates, it gives estimates of γ_{loc} which agree very closely with the values from the finite element program. The agreement is due, in part, to use here of a relatively diffuse temperature

17

perturbation and large $\frac{\cdot}{\gamma_o}$, both of which tend to reduce the effect of heat conduction. Note also that Wright's scheme handles cases in which the integral in Equation (45) diverges.

For $m \ll 1$, Wright uses an asymptotic analysis to show that his estimate of γ_{loc} depends on g primarily through the softening parameter which for an arbitrary softening variant is defined by $a = -g'(0)$. That is, given several different g's for which a takes the same value, prior to severe localization, the parametric solution is approximately independent of the particular g. He also shows that γ_{loc} must be proportional to $a/m = \chi_{sb}$, which he terms the *shear band susceptibility*. Moreover, for a sufficiently small perturbation (i.e., $\max_{0<y<1}\theta_i(y)\,(a/m) \ll 1$) of simple shape

$$\theta_i(y) = \varepsilon \cos(\pi y) , \tag{46}$$

and in the locally adiabatic case, Wright obtains the explicit estimate

$$\gamma_{loc} = \frac{mC}{a} \ln\left[\frac{1 + \sqrt{1 - \delta^2}}{\delta}\right] \approx \frac{mC}{a} \ln\left(\frac{2}{\delta}\right), \quad \delta = \frac{\varepsilon a}{m} . \tag{47}$$

Note that this result depends on g only through a and the parameter C which is of order $1 + O(m)$ and which depends weakly on the overall shape of g. As may be seen in Table 3, C varies in accord with γ_{loc} although the magnitude of variation is smaller than needed to account for the variation of γ_{loc} in Table 2.

Molinari and Clifton (1987, Equation [33]) also obtain an estimate for the point-wise strain $\gamma^c(y)$ at severe localization. Using variables introduced here, for flow law (Equation [43]$_1$) and with perturbation (Equation [46]), their estimate of γ_{loc} follows as

$$(\gamma_{loc})_{MC} = \int_0^1 \gamma^c(y)dy = \int_0^1 \frac{e^{\varepsilon a \cos \pi y}}{a}\left[\left(1 - e^{-2\varepsilon a(1 - \cos \pi y)\frac{1-m}{m}}\right)^{-\frac{m}{1-m}} - 1\right]dy . \tag{48}$$

Table 3. Variation of Shape Parameter "C" Appearing in Equation (47)

Softening Variant	g_1	g_2	g_3	g_4
C	0.973	0.976	1	1.03

Note that as in the locally adiabatic form of Wright's scheme for a RPP material (used to obtain Table 2), Equation (48) really involves two quadratures: one to obtain $\gamma^c(y)$ and the other as shown. For the material constants in Table 1 and $\varepsilon = 0.1$, Wright's scheme yields $(\gamma_{loc})_{Wright} = 0.299$, Equation (48) yields $(\gamma_{loc})_{MC} = 0.316$, and the finite element value is $(\gamma_{loc})_{fem} = 0.305$. While $(\gamma_{loc})_{Wright}$ and $(\gamma_{loc})_{MC}$ each follow from a locally adiabatic analysis, and so should provide a lower bound to $(\gamma_{loc})_{fem}$, only the former does. The difficulty in the latter case seems to lie in the use of the nominal rather than local strain rate in the flow law to obtain an expression for the stress (Molinari and Clifton 1987, Equation [29]). In the current notation, this approximation is $s \approx g(\theta(y,t))$, while the exact result for flow law (Equation [43]$_1$) is $s = \left(\int_o^1 g(\theta(y,t))^{-1/m} \, dy \right)^{-m}$, as shown by Wright (1990b). The error incurred by the approximate stress depends on the extent to which θ has localized (in the FEM solution) when $\gamma_o = (\gamma_{loc})_{MC}$.

4.2. Elastic Effects in the Perfectly Plastic Case.
In this section, we illustrate a coupling between the basic localization mode of the previous section and the elastic response of the material. We consider the same IBVP for the same flow law with softening variant g_3 as given by Equation (12)$_3$. First, Figure 12 shows a full-field view of the velocity in the *rigid* case for a range of γ_o containing γ_{loc}; note the orientation of the base plane axes and the log scale in y. Restoring the elastic modulus μ to the value listed in Table 1 produces the result shown in Figure 13. The effect of the elastic energy stored in the slab is nontrivial in that the velocity in the elastic case overshoots that in the rigid case by nearly 40%. Figure 14 shows that, in spite of the substantial overshoot in velocity, the localization remains approximately quasi-static as the stress gradient $\partial s/\partial y$ is too small to be seen at this scale. In Figure 15, where the central values of $\dot{\gamma}_p$, θ, and s for both cases are superimposed, we see that in the

19

elastic case localization occurs slightly earlier, with a slightly stronger stress drop and temperature increase, and a considerably stronger increase in $\dot{\gamma}_p$ in accord with the overshoot in v. In all cases, however, the deviations from rigid response are rapidly damped and the elastic response decays back to the rigid case.

To probe the effect of varying the nominal strain rate, elastic computations identical to those just described were performed at $\dot{\overline{\gamma}}_o = 750/s$. The results in the rigid case are similar to those at the lower value of $\dot{\overline{\gamma}}_o$, although the localization is a little more severe. For example, comparing Figures 15 and 16, the peak value of $\dot{\gamma}_p$ in the rigid case increases about 50% in proportion to the change in $\dot{\overline{\gamma}}_o$, as observed by Wright and Walter (1987). In contrast, the elastic effects are much stronger at the higher rate (e.g., the maximum overshoot in velocity [not shown] is more than twice as large). Referring to Figure 16, the maximum value of the ratio $(\dot{\gamma}_p(0,t)_{elastic})/(\dot{\gamma}_p(0,t)_{rigid})$ is about 5 at $\dot{\overline{\gamma}}_o = 750/s$ as compared with 1.5 at $\dot{\overline{\gamma}}_o = 500/s$. Moreover, as indicated in Figures 17 and 18, the temperature and stress show strong temporal oscillations, whereas at the lower $\dot{\overline{\gamma}}_o$, these oscillations are too small to be seen on top of the underlying rigid response. The degree to which the shear band serves to concentrate the stored elastic energy is made clear by observing that the prelocalization, stored elastic energy would produce a temperature increase of about 1° C if converted completely and adiabatically to heat. In contrast, the maximum difference in central temperatures $\theta_{elastic} - \theta_{rigid}$ is about 275° C. Note also that the stress in the elastic case $(\dot{\overline{\gamma}}_o = 750/s)$ shows a mild spatial gradient indicating that wave propagation effects are beginning to become important. This is in contrast to earlier results (*ibid*) which for the same RPP material model (but with thermal softening variant g_2) and the same IBVP indicate that wave propagation does not become important until $\dot{\overline{\gamma}}_o$ exceeds 5,000/s–10,000/s.

The effects just described are certainly driven by the release of stored elastic energy upon severe localization but the explanation for the strong increase in their magnitude with $\dot{\overline{\gamma}}_o$ is more subtle. With the increase in nominal rate, there is an increase in prelocalization stress, but the factor is only $(1.5)^m \approx 1.01$ (where m is the strain rate hardening exponent) and so cannot account for the observed difference. Part of the increased magnitude may be

20

attributed to more intense localization in the underlying rigid case. Referring to Figures 15 and 16, the maximum rate of stress collapse is larger at $\dot{\gamma}_o$ = 750/s and (after accounting for the difference in γ_{loc} by shifting the 750/s stress curve to the left by $\Delta\gamma_o$ = 0.05) the stress drop over the γ_o-interval from 0.2725 to 0.2925 (Figure 16) is 20–25% larger than the corresponding drop at $\dot{\gamma}_o$ = 500/s. Since the elastic energy is proportional to s^2, it follows that 15–20% more stored energy is available to drive the shear band at 750/s than at 500/s. Moreover, as noted by Wright and Walter (1987), the band width w_{sb} in the rigid case is inversely proportional to $\dot{\gamma}_o$ in the range from $\approx$ 10/s to $\approx$ 10^4/s. Thus, based on comparison of the rigid cases alone, an intensification of 70–80% is to be expected in the elastic case at the higher rate. Of course, the situation is really more complex than this since the flow of stored energy into the core of the shear band is *autocatalytic* in that it dynamically intensifies the stress drop which, in turn, releases more energy. Moreover, for $\dot{\gamma}_o$ in the range considered, the elastic wave speed is sufficiently large so that stress changes produced at the band core propagate to the slab boundary very rapidly compared to the stress rate at the core. For example, at 750/s, the nominal strain increment needed for an elastic wave to traverse the slab is $\Delta\gamma_o \approx 8(10^{-4})$. Consequently, in the cases discussed here, elastic wave propagation does not limit the rate at which stored elastic energy flows into the shear band. Once the initial localization has occurred, the unloaded outer portions of the slab (comprising almost all the thickness) execute essentially a free oscillation with the shear band acting as a sort of thermo-visco-plastic damper.

In a related study, Batra and Kim (1990) examined the same IBVP for a flow law similar to that employed here (work hardening was included)—the same material parameters but with an artificially large thermal softening coefficient and a linear thermal softening factor as in Equation (12)$_2$. Even though the nominal strain rate was only 500/s, they observed, upon occurrence of severe localization, a well-defined elastic unloading wave propagate from the center of the slab and reflect from the outer boundary, presumably because of the very strong thermal softening they used. They also observed a large overshoot in the nondimensional velocity (values as large as 15) and some oscillation in the plastic strain rate. The computed speed of propagation of the unloading wave agreed very closely with the elastic shear wave speed. Their observations are consistent with those reported here and, had their computation

been continued to larger nominal strains, it seems likely that thermo-visco-plastic oscillations, of the sort noted here, would have ensued. Further numerical study regarding the dependence of the elastic effects on various parameters and the boundary conditions is warranted.

4.3. Simulation of a High Rate Torsion Test.

In this section, the flow law of Johnson and Cook (1983) is used to simulate a torsion test on OFHC copper as reported by Lindholm et al. (1980) and analyzed by Johnson (1981). The Johnson-Cook law is in the form of Equation (11), with $\kappa(\psi)$ and $f(\dot{\gamma}_p)$ given by Equations (13) and (14)$_2$, respectively, and $g(\theta)$ taking one of several forms depending on the material (Johnson 1983a, 1983b). In this case, $\kappa(\psi)$ describes the isothermal plastic stress-strain curve at a reference strain rate of $\dot{\gamma}_o = 1/s$, and setting $b = 1$ in Equation (14)$_2$, ensures consistency with this interpretation of κ. The tests reported by Lindholm et al. (1980) cover a range of nominal strain $0 < \gamma_o < 7$ and a range of nominal strain rate $0.009/s < \dot{\gamma}_o < 330/s$. The isothermal flow law parameter values used for the simulations reported by Johnson (1981) were obtained by curve-fitting to Lindholm's data but only for $\dot{\gamma}_o \le 9.6/s$ because of thermal softening at the higher rates. Johnson suggests a bi-linear form for the thermal softening factor g based on static experiments performed by Hawkyard et al. (1968) at nominal strain $\gamma_o = 0.9$. To roughly approximate this data with a smooth function, we use here $g(\theta) = (1 - a\theta)^p$ with $1/a = \theta_{melt}$ and $p = 3$. Lastly, note that we use ψ as the strain hardening variable, which evolves according to Equation (4), whereas Johnson used $\gamma_p = \int^t |\dot{\gamma}_p| \, dt$. Thus, even though we use the same parameter values and give the same interpretation to the right side of Equation (14)$_2$, our isothermal flow law is not identical to his.

The torsion specimen used in Lindholm et al. (1980) has a gauge length of 3.18 mm with a wall thickness of 0.79 mm, while the included angle between the gauge length and the transition to the specimen shoulder is 119°. Consequently, it is an acceptable approximation to ignore any loss of heat along the lateral surface and to assume that the shoulders act as rigid, isothermal heat sinks. The dimensional material constants obtained from Johnson et al. (1983a) appear in Table 4 and the thickness $\bar{h} = 1.59$ mm used in the computation corresponds to one-half the gauge length. The model problem considered here ignores multidimensional aspects of the experiment such as axial normal stresses and strains and radial or circumferential nonuniformity as the shear band grows. These and other features of

22

thin-wall tube experiments may, of course, have significant effects on observed results (Hartley et al. 1987; Marchand and Duffy 1988).

The specific IBVP considered here corresponds to the fastest experiment reported in Lindholm et al. (1980) for which $\dot{\gamma}_o$ = 330/s; the results appear in Figures 19–26. To model this experiment, uniform initial conditions

$$v_{iy}(y) = 1, \quad \theta_i(y) = 0, \quad \psi_i(y) = 0, \quad s_i(y) = 1 + m\log(b), \qquad (49)$$

are used along with boundary conditions (Equations [19] and [21]). In contrast to the cases in the previous two sections, no perturbation is introduced here. Initially, $\dot{\theta}$ is uniform and $\theta_{yy} = 0$ for $y \in (0,1)$. As θ increases in the interior, a thermal boundary layer develops at $y = 1$ which gradually diffuses toward the center as may be seen in Figures 19 and 25. Note that the stress remains uniform in y (Figure 20) and that, in spite of strong strain hardening at small nominal strains (Figure 22), plastic flow has almost ceased for $y \gtrsim 0.7$ by the time $\gamma_o = 2$ (Figure 26).

Burns (1990) has studied the early stages of this thermal boundary layer mechanism for shear band formation and concludes that when the dimensionless thermal conductivity is sufficiently large, a single central shear band is to be expected, as occurs here at $\gamma_o = 2$. This mode of localization is quite different from that which occurs from perturbation of a homogeneous solution. In particular, strain rate localization begins during the initial rapid stress increase (when $\gamma_o < 1$), whereas for the perturbed homogeneous problem $ds/d\gamma_o > 0$ signifies (at least temporary) stability in the strain hardening case.[*]

---

[*]General conditions ensuring the infinitesimal stability or instability of a strain-hardening homogeneous solution have not yet been determined. Elementary criteria, such as are relevant to constant coefficient systems of ordinary differential equations, do not apply. As an example, Hale (1980, Example 7.1) cites a specific linear, *nonconstant* coefficient, second-order system (of the form $\dot{x}(t) = A(t)x(t)$ in which the $A_{ij}(t)$ are sinusoids. $A(t)$ has two distinct, constant, eigenvalues both of whose real parts are strictly negative. Were A *itself* constant with the same eigenvalues, then all solutions of the system would decay exponentially. Nonetheless, Hale shows that for the given there are solutions which *grow* exponentially at all times. The shear band problem is, of course, far more complex than this example and much deeper analyses are needed.

In this connection, Wright (1990a, 1992) has shown that strain hardening introduces a *temporal boundary layer* into the solution of the linearized perturbation equations so that their initial behavior is *not* representative of their behavior at slightly later times. Following this boundary layer, it is also possible for perturbations to grow briefly but then to decay and so *not* lead ultimately to localization.

The initial localization in this case is driven by propagation of the thermal boundary layer and will occur with or without strain hardening. A less obvious consequence of strain hardening is the subsequent complex interaction of the various fields. Computation for an effectively rigid version of the same problem indicates that at this nominal strain rate elastic energy release has almost no effect on the solution. To interpret the solution features that develop, it is easiest to follow the $\dot{\gamma}_p$ curve on Figure 23. Following the initial peak at $\gamma_o = 2.2$, there is a subsequent decay followed by another peak at $\gamma_o = 4.2$. The pattern then repeats much more strongly for $4.2 < \gamma_o < 7$. Referring to Figures 19–23, the $\dot{\gamma}_p$ peak at $\gamma_o = 4.2$ is accompanied by a slightly delayed peak in θ, a valley in s (at $\gamma_o = 4.6$), and a rapid increase in ψ. This sets the stage for the collapse of the $\dot{\gamma}_p$ peak; recall that $\dot{\gamma}_p$ is an increasing function of s but a decreasing function of θ and ψ. Once the θ profile is sufficiently localized, diffusion begins to slow its growth but the magnitude of strain hardening $\psi(0,\gamma_o)$ at the slab center increases while s decreases so that $\partial \dot{\gamma}_p(0,\gamma_o)/\partial \gamma_o$ also decreases. Thermal diffusion also causes softening of the material at larger y with a corresponding increase in $\dot{\gamma}_p$ there. This forces $\dot{\gamma}_p(0,\gamma_o)$ to decrease because $\int_o^1 \dot{\gamma}_p \, dy$ is conserved in view of Equations (19₁) and (20₁). As $\dot{\gamma}_p(0,\gamma_o)$ begins to decrease, so does heat production which accelerates the decay of $\dot{\theta}$ causing θ to peak and then decay. Thus, *thermal* hardening due to cooling is added to the strain hardening accumulated previously which drives $\dot{\gamma}_p(0,\gamma_o)$ almost to zero even though s increases concurrently (due to work and strain rate hardening which occur farther out in the slab).

The sharp peak in $\dot{\gamma}_p$ at $\gamma_o = 7$ occurs by roughly the reverse of the process just described. For $0 \leq y \leq 0.1$ and $6.3 \leq \gamma_o \leq 6.7$, θ_{yy} is very slightly positive (due to heat production farther out in the slab) so no heat is lost from the center during this period. The stress continues to increase until $\gamma_o = 6.5$ but no strain hardening occurs near $y = 0$ until $\gamma_o = 6.7$. Hence, $\dot{\gamma}_p$ and θ begin to increase simultaneously at $\gamma_o = 6.2$ with weak strain rate hardening initially being the only effect to balance the stress increase and thermal softening. The strain hardening which begins to accumulate later in the localization reduces the magnitude of stress drop (compared to the RPP response) and so actually intensifies the

24

localization. Although not shown in the figures, this computation was carried until γ_o = 15 with the pattern of irregular oscillation showing no sign of abating.

The only time history reported (Lindholm et al. 1980; Johnson 1981) for the relevant test is a curve of stress against nominal strain. The experimental stress $\bar{s}$ increases rapidly until a fairly sharp knee at γ_o = 0.5 continues to rise slowly for $0.5 < \gamma_o < 2$, more rapidly for $2 < \gamma_o < 3$, varies little for $3 < \gamma_o < 5$ with a mild peak of $\bar{s}$ = 0.21 GPa at γ_o = 4, and then decays rapidly to $\bar{s}$ = 0.15 GPa between $5 < \gamma_o < 7$. Postmortem examination of the specimen (Lindholm et al. 1980) revealed considerable surface necking centered around the shear band so that fracture was judged to be imminent. The maximum stress on Figure 23 ($\bar{s}$ = 0.18 GPa at γ_o = 1) is quite close to the experimental value at the same γ_o (Johnson 1981, Figure 9) indicating that the early strain hardening of the material is modeled accurately. However, at larger strains, our computed stress consistently lies below the experimental value and fluctuates more rapidly. The same computation has been performed with different values of the thermal softening factor exponent: $p = 2$ and $p = 1.5$. The solution structures are qualitatively similar to the $p = 3$ case, except that the various fluctuations occur more slowly and are less severe. The stress levels are generally higher and the locations of the initial peaks are delayed considerably. For $p = 1.5$, s decays slightly after an initial peak at γ_o = 3 and does not peak again until well after the experiment had stopped. Of the three cases calculated here, $p = 2$ gives a stress history which agrees most closely with the Johnson's EPIC-2 simulation of the experiment (ibid) but none of the calculations did a particularly good job of reproducing the shape of the stress history.

The shape of the experimental curve (ibid) suggests that a flow law with stronger strain hardening for $\gamma_o > 1$ would bring the simulated stress closer to that of the experiment. From Equations (6), (11), and (15)$_4$, it follows that $\dot{\psi}/\dot{\gamma}_p = g(\theta) f(\dot{\gamma}_p)$ so that γ_p exceeds ψ after just a little thermal softening has occurred, as may be observed in Figure 24. Use of γ_p rather than ψ (with the same material constants) would increase the degree of isothermal strain hardening. For example, substitution of the values of ψ and γ_p at γ_o = 6 on Figure 24 into Equation (16)$_2$ gives 4.21 and 4.58, respectively. However, increased plastic work also leads to increased softening and so partially offsets the larger isothermal stresses; viz. the net effect of using γ_p (ibid) was not sufficient to reproduce the shape of the stress history accurately. It

25

seems clear that what is really needed is a more refined functional form of the flow law fit to experimental data over a much wider range of the constitutive variables. Of course, the thin-wall tube is not the best geometry for obtaining constitutive data at very large strains. However, it is a good test for determining the modeling efficacy of a high rate flow law because, assuming a specimen of sufficiently "clean" material, shear localization can be initiated by thermal boundary layer diffusion or by wall thickness variation rather than by material defects whose strength is far harder to quantify.

5. DISCUSSION

The intent of this research has been to explore the behavior of a system of field equations which describes some aspects of adiabatic shear band formation in one space dimension. One of the most important observations is that shear band formation can drive the material into extreme ranges of strain, strain rate, and temperature. This is especially true in the context of ballistic penetration, because there shearing deformations may be accompanied by large pressures which can delay fracture until extremely large strains have accumulated at the band core. For example, when thin-wall tube torsion tests are performed on a tungsten heavy alloy (WHA), actually a metal-particle/metal-matrix composite (Coates and Ramesh 1990), some shear localization may occur before fracture. However, local shearing of the tungsten particles is *much* less severe than that which is observed in a WHA penetrator remnant impacted at ordnance velocities. In a more quantitative example, Moss (1981) performed plug punching experiments on an armor steel whose microstructure contained "reference bands" (planes of chemical inhomogeneity) which were oriented perpendicularly to the direction of plugging. The reference bands were clearly visible inside the "transformed" shear band which formed at the plug boundary to within about 4 μm of the edge. The local strain in the shear band was computed from the rotation of the reference bands. Moss judged that the shear strain varied exponentially with distance from the transformation interface, that the maximum strain was greater than 500 and that the maximum strain rate approached 10^8/sec. No pressure was applied other than that produced by the punch, whose velocity was 20 m/sec.

Based on this experimental evidence and results presented here, several general observations may be made. First, shear band formation need *not* be followed immediately by fracture or complete loss of strength (Section 4.3); exactly when either ensues depends

strongly on loading (i.e., pressure) and material microstructure. This implies that *post-localization* modeling of individual bands is an essential step in the development of phenomenological models for the various effects of shear bands on a material's mechanical response. The shear band kinetics and post-localization morphology in the problem considered here depend strongly on the underlying homogeneous flow response of the material. Consequently, there is a need for constitutive data and thermo-visco-plastic flows laws which are valid over a very wide range of strain, strain rate, temperature, and pressure. Although probably unavoidable, application of constitutive data and flow laws obtained from low-rate, low-pressure experiments to shear band simulation may lead to spurious conclusions (Clifton 1990).

Building on Wright and Walter (1987) and motivated by Wright (1990b), the effect of *qualitative* variation in the strength of thermal softening was considered analytically in Section 3 and numerically in Section 4.1. An important result was to verify that Wright's parametric solution scheme (*ibid*) can provide an excellent estimate for the nominal strain at which shear banding occurs. It was also shown that, depending on material behavior, some aspects of shear band formation may be *transient* (*viz.* the decay of strain rate localization). Consequently, analytical localization criteria which emphasize the long-time behavior of the model problem may lead to spurious conclusions.

Calculations in the elastic perfectly plastic case showed how the shear band can act to concentrate in the band core the elastic energy stored in the rest of the domain and so enhance the severity of the localization process. The elastic effects may be quite strong even though the stored energy density is small, and they depend strongly on the severity of the underlying localization process.

Simulation of a moderately high-rate torsion test of OFHC copper revealed that strain hardening can add complex, nonperiodic structure to the morphology, even when elastic and inertial effects are unimportant. In this case, localization occurred on a length scale roughly 100 times larger than in the previous cases showing principally the effect of greatly increased thermal conductivity and reduced heat production due to the much lower flow stress in this material. This simulation also showed how localization can be initiated by thermal boundary layer propagation in the absence of any other perturbation.

Another concern is the concept of the width of a shear band. For the particular case of linear thermal softening with the flow law used here, a time-independent, post-localization band width can be defined because the spatial profiles of velocity and plastic strain rate become asymptotically constant following rapid localization. However, even in this case the temperature profile continues to evolve after localization. For any other thermal softening behavior, the post-localization profile of plastic strain rate will also continue to evolve, more or less rapidly as determined by its deviation from linear thermal softening. When elasticity, strain hardening, or inertial effects are added, the picture may become much more complicated. Hence, there are at least two and perhaps several time-dependent "widths" for a shear band. Exactly which bandwidth should be compared with an experimental measurement or a different calculation is a matter for case-by-case consideration.

The minimal finite element method employed here has proved adequate in the cases presented but more sophisticated methods are needed to fully explore these field equations. Careful initial mesh refinement and a very small temporal integration error tolerance had to be used at times. Error control problems were most severe for the elastic cases of Section 4.2. Since spatial discretization errors were not controlled, some simulations attempted could not be performed satisfactorily. The initial mesh and other parameters controlling the numerical solution were varied in each case reported to obtain results (hopefully) independent of these quantities, but questions of accuracy remain. When the location of large gradients cannot be predicted a priori, adaptive meshing of some sort becomes essential to obtain complete results at reasonable computational expense.

Although this one-dimensional problem has been much studied numerically in recent years (most extensively by Batra and co-workers [Batra 1987, 1989; Batra and Kim 1987, 1988, 1990; Batra and Wright 1988]), its parameter space is far from completely explored, even qualitatively. Effects of combined shear and compression, of particular relevance to ballistic applications, have scarcely been addressed as is the case for possible effects of phase transitions or a transition in dislocation-drag controlling mechanism. With sufficiently robust and efficient numerical techniques, systematic mapping of the parameter space will allow determination of scaling laws for quantities such as localization strain and magnitude of stress collapse during localization which are needed in order to develop a damage mechanics for

shear bands. Lastly, it seems likely that understanding of more complex two- ar three-dimensional shear band problems will be enhanced by the solution of appropriate one-dimensional subproblems.

INTENTIONALLY LEFT BLANK.

6. REFERENCES

Batra, R. C. "The Initiation and Growth of, and the Interaction Among Adiabatic Shear Bands in Simple and Dipolar Materials." International Journal of Plasticity, vol. 3, p. 75, 1987.

Batra, R. C. "Effect of Nominal Strain Rates on Adiabatic Shear Banding in Dipolar Materials." Proceedings of the Pan American Congress of Applied Mechanics, Rio de Janeiro, pp. 79–82, 1989.

Batra, R. C., and C. H. Kim. "On the Interaction Among Adiabatic Shear Bands." W. Soedel and J. F. Hamilton (ed.), Developments in Mechanics, Purdue University, pp. 117–122, 1987.

Batra, R. C., and C. H. Kim. "Effect of Material Characteristic Length on the Initiation, Growth, and Band Width of Adiabatic Shear Bands in Dipolar Materials." Journal of Physics, (Paris), vol. 49, p. 41, 1988.

Batra, R. C., and C. H. Kim. "Adiabatic Shear Banding in Elastic-Viscoplastic Nonpolar and Dipolar Materials." International Journal of Plasticity, vol. 6, p. 127, 1990.

Batra, R. C., and T. W. Wright. "A Comparison of Solutions for Adiabatic Shear Banding by Forward-Difference and Crank-Nicolson Methods." Communs. Appl. Numer. Meths, vol. 4, p. 741, 1988.

Becker, E. B., G. F. Carey, and J. T. Oden. Finite Elements: An Introduction. Vol. 1, Englewood Cliffs, NJ: Prentice-Hall, 1981.

Burns, T. J. "A Mechanism for Shear Band Formation in the High Strain-Rate Torsion Test." Journal of Applied Mechanics, vol. 57, p. 836, 1990.

Clifton, R. J. "High Strain Rate Behavior of Metals." Appl. Mech. Revs, vol. 43 (5), p. S9, 1990.

Coates, R. S., and K. T. Ramesh. "The Deformation of Tungsten Alloys at High Rates of Strain." Technical Report DIL-9002, The Johns Hopkins University, Baltimore, MD, 1990.

Frohlich, C. "Deep Earthquakes." Scient. Am., vol. 260 (1), p. 48, 1989.

Gear, C. W. Numerical Initial Value Problems in Ordinary Differential Equations. Englewood Cliffs, NJ: Prentice-Hall, 1971.

Hale, J. K. Ordinary Differential Equations, second edition, Malabar, FL: Krieger.

Hartley, K. A., J. Duffy, and R. H. Hawley. "Measurement of the Temperature Profile During Shear Band Formation in Steels Deforming at High Strain Rates." Journal of Mech. Phys. Solids, vol. 35 (3), p. 283, 1987.

Hawkyard, J. B., D. Eaton, and W. Johnson. "The Mean Dynamic Strength of Copper and Low Carbon Steel at Elevated Temperatures From Measurements of the Mushrooming of Flat-Ended Projectiles." International Journal of Mech. Sci., vol. 10 (12), p. 929, 1968.

Hindmarsh, A. C. "ODEPACK, a Systematized Collection of ODE Solvers." R. S. Stepleman, et al. (ed.), Scientific Computing, North-Holland, IMACS, pp. 55–64, 1983.

Johnson, G. R. "Dynamic Analysis of a Torsion Specimen Including Heat Conduction and Plastic Flow." ASME Journal of Engineering Material Technology, vol. 103, p. 201, 1981.

Johnson, G. R., and W. H. Cook. "A Constitutive Model and Data for Metals Subjected to Large Strains, High Strain Rates, and High Temperatures." Proceedings of the Seventh International Symposium on Ballistics, The Hague, The Netherlands, pp. 541–548, 1983.

Johnson, G. R., J. M. Hoegfeldt, U. S. Lindholm, and A. Nagy. "Response of Various Metals to Large Torsional Strains Over a Large Range of Strain Rates–Part 1: Ductile Metals." ASME Journal of Engineering Material Technology, vol. 105, p. 42–47, 1983a.

Johnson, G. R., J. M. Hoegfeldt, U. S. Lindholm, and A. Nagy. "Response of Various Metals to Large Torsional Strains Over a Large Range of Strain Rates–Part 2: Less Ductile Metals." ASME Journal of Engineering Material Technology, vol. 105, p. 48–53, 1983b.

Johnson, W. "Henri Tresca as the Originator of Adiabatic Heat Lines." International Journal of Mech. Sci., vol. 29, p. 301, 1987.

Lindholm, U. S., A. Nagy, G. R. Johnson, and J. M. Hoegfeldt. "Large Strain, High Strain Rate Testing of Copper." ASME Journal of Engineering Material Technology, vol. 102, pp. 376–381, 1980.

Litoński, J. "Plastic Flow of a Tube Under Adiabatic Torsion." Bull. Acad. Pol. Sci., vol. 25 (1), p. 1, 1977.

Marchand, A. and J. Duffy. "An Experimental Study of the Formation Process of Adiabatic Shear Bands in a Structural Steel." Journal of Mech. Phys. Solids, vol. 36 (3), p. 251, 1988.

Molinari, A. and R. J. Clifton. "Analytical Characterization of Shear Localization in Thermoviscoplastic Materials." Journal of Applied Mechanics, vol. 54, p. 806, 1987.

Moss, G. L. "Shear Strains, Strain Rates, and Temperature Changes in Adiabatic Shear Bands." M. A. Meyers and L. E. Murr (ed.), Shock Waves and High-Strain-Rate Phenomena in Metals, Plenum Press, pp. 299–312, 1981.

Tresca, H. "On Further Applications of the Flow of Solids." Proceedings Instn Mech. Engrs, vol. 30, p. 301, 1978.

Tzavaras, A. E. "Shearing of Materials Exhibiting Thermal Softening or Temperature Dependent Viscosity." Q. Appl. Math., vol. XLIV (1), p. 1, 1986.

Wright, T. W. "Adiabatic Shear Bands." Appl. Mech. Revs, vol. 43 (5), p. S196, 1990a.

Wright, T. W. "Approximate Analysis for the Formation of Adiabatic Shear Bands." Journal of Mech. Phys. Solids, vol. 38 (4), p. 515, 1990b.

Wright, T. W. "Shear Band Susceptibility: Work Hardening Materials." To appear in International Journal of Plasticity, 1992.

Wright, T. W., and R. C. Batra. "The Initiation and Growth of Adiabatic Shear Bands." International Journal of Plasticity, vol. 1, p. 205, 1985.

Wright, T. W., and J. W. Walter, Jr. "On Stress Collapse in Adiabatic Shear Bands." Journal of Mech. Phys. Solids, vol. 35 (6), p. 701, 1987.

Zener, C., and J. H. Holloman. "Effect of Strain Rate Upon Plastic Flow of Steel." Journal of Appl. Phys., vol. 15, p. 22, 1944.

$$\dot{\gamma}_0 = 5.000(10^2)/\text{s}$$
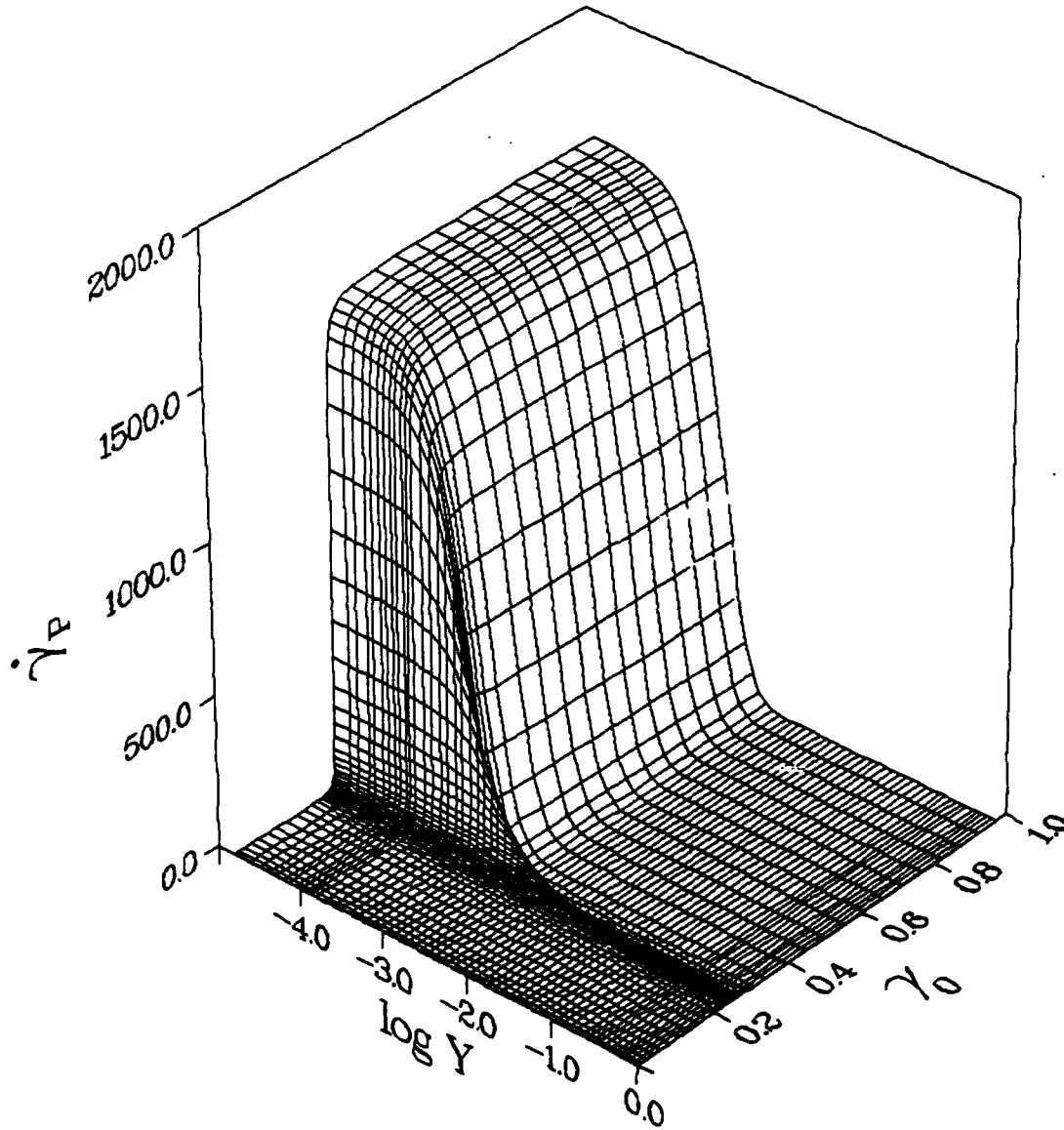
Note: The logarithmic axis in y is necessary to resolve the severe localization.

Figure 1. Plastic Strain Rate Surface at $\dot{\gamma}_o$ = 500/s for the Rigid, Perfectly Plastic, Linear Thermally Softening Material Model ($g = g_2$).
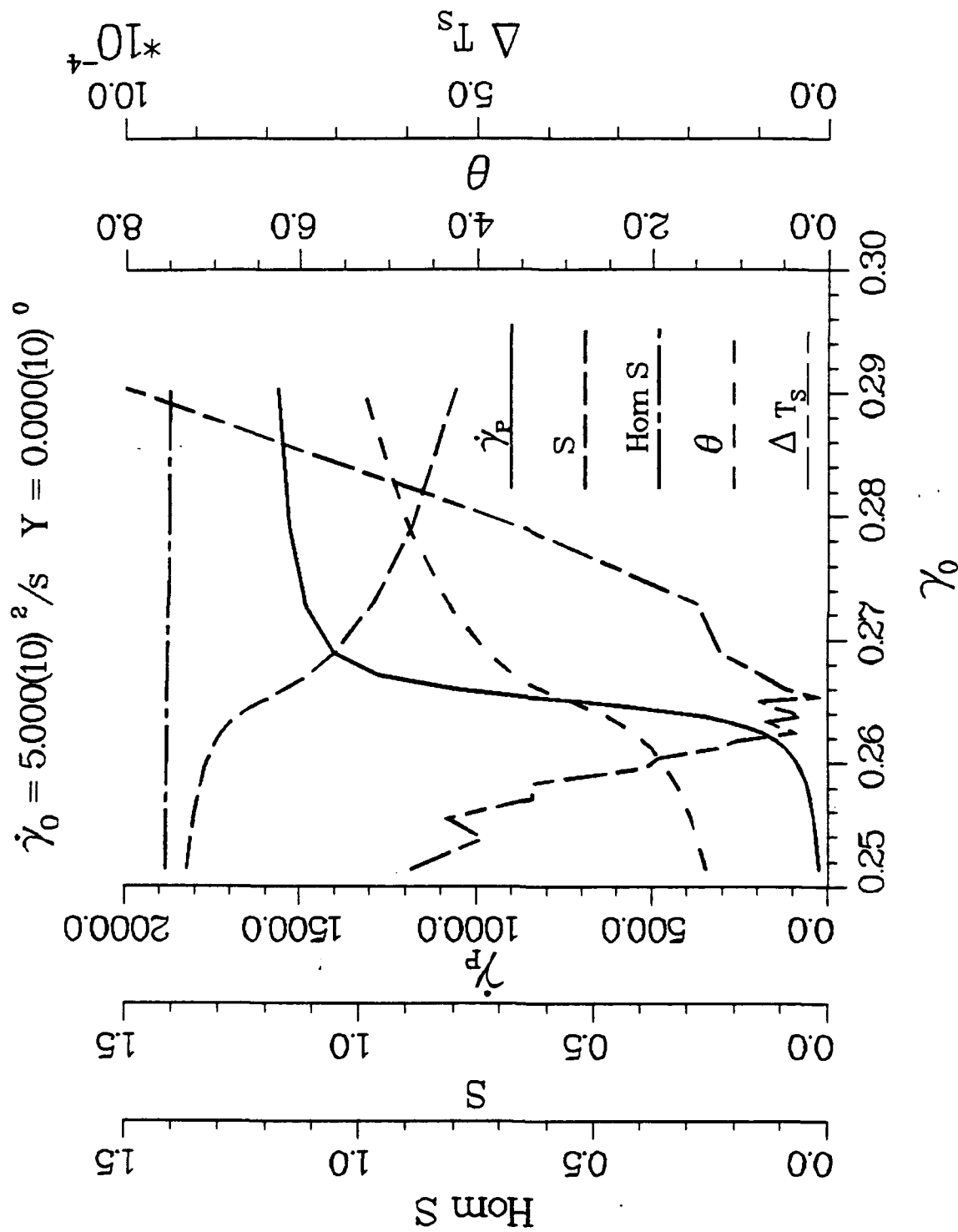
Note: The numerical time step and stress for the homogeneous solution are also indicated.

Figure 2. Plastic Strain Rate, Temperature, and Stress at y = 0 for the Case of Figure 1.

$$\dot{\gamma}_0 = 5.000(10^2)/s$$
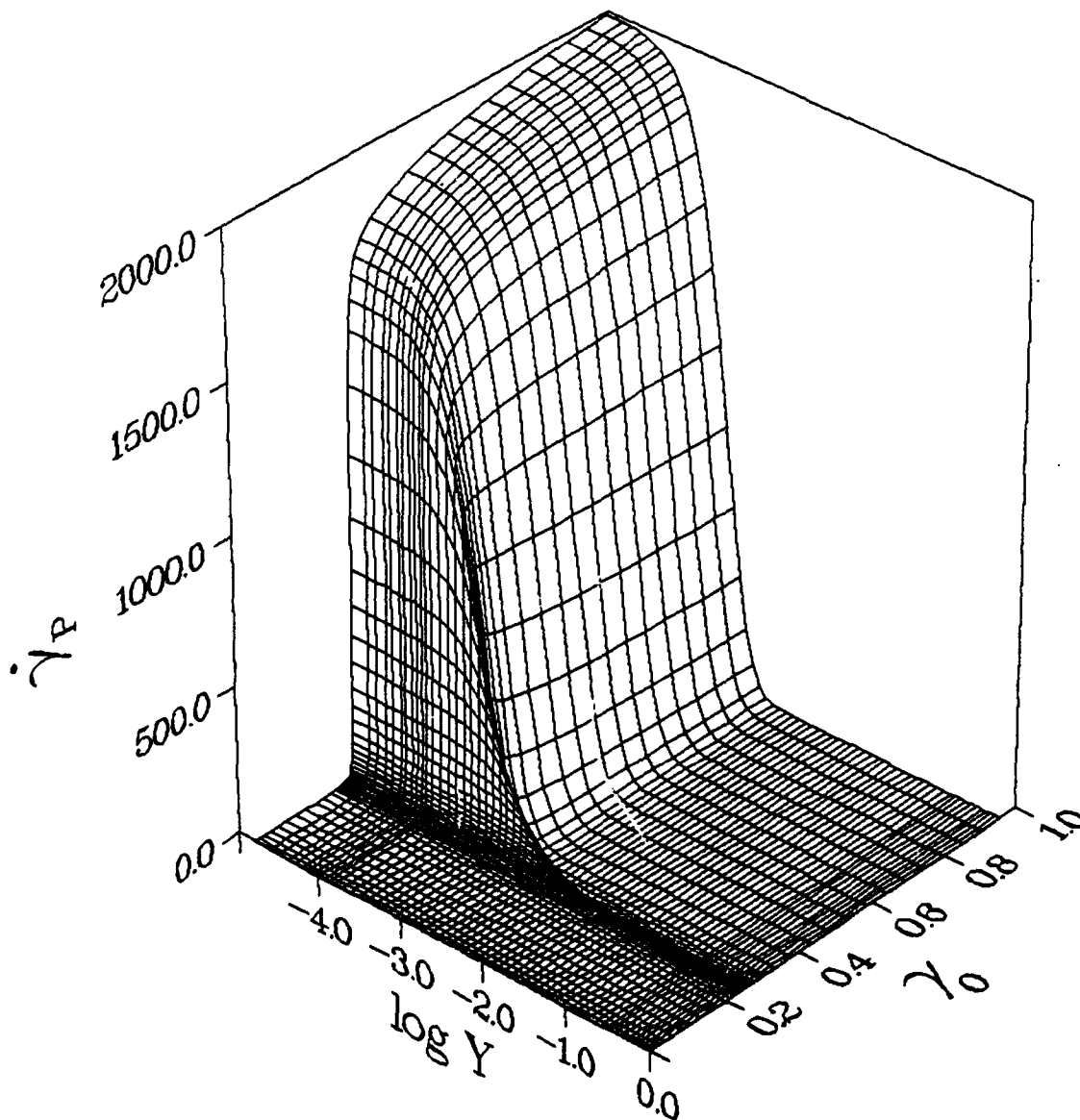
Figure 3. Plastic Strain Rate Surface at $\dot{\overline{\gamma}}_o$ = 500/s for Softening Variant g_1.

$$\dot{\gamma}_0 = 5.000(10^2)/s$$
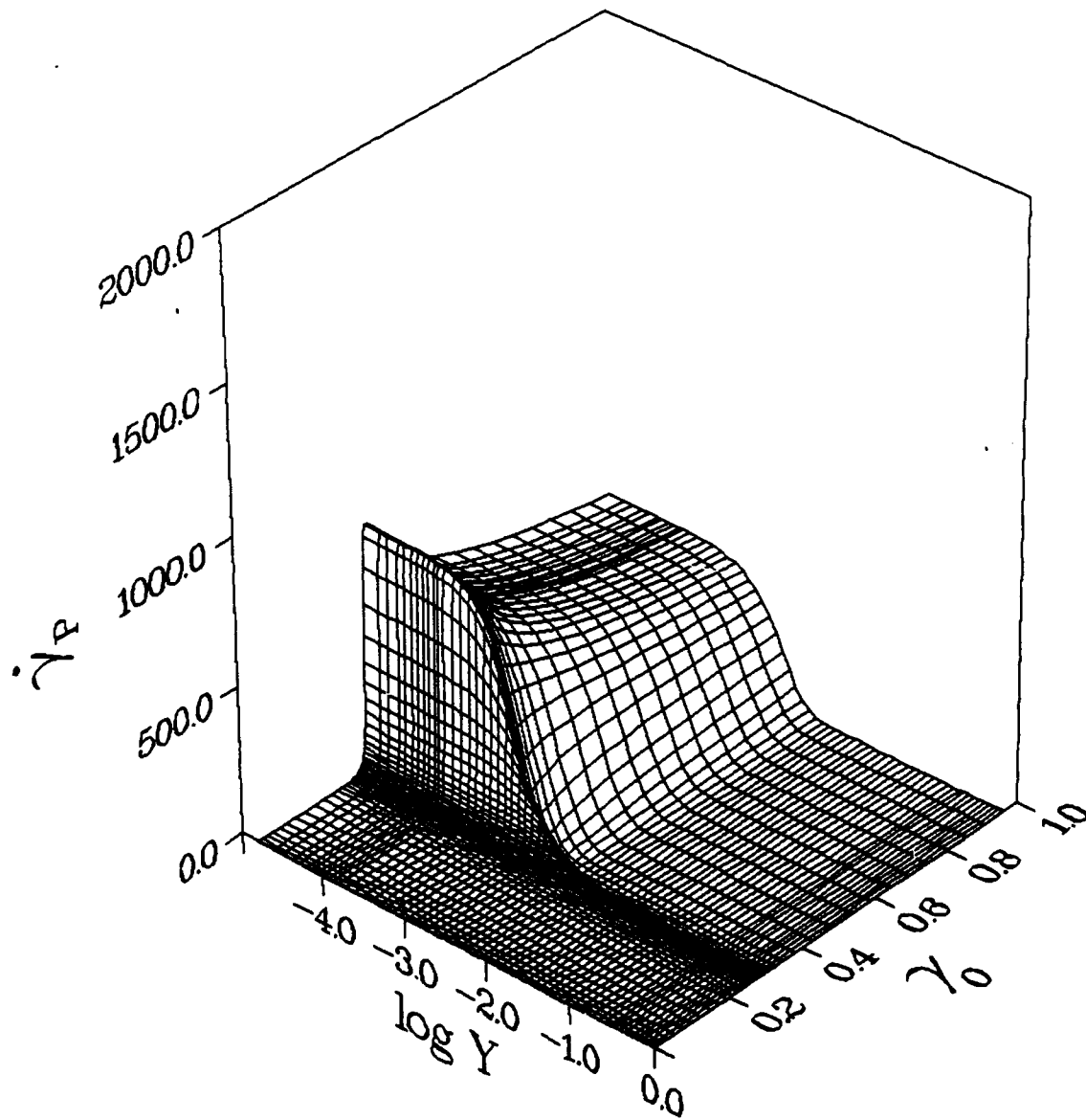
Figure 4. Plastic Strain Rate Surface at $\dot{\bar{\gamma}_o}$ = 500/s for Softening Variant g_3.

$$\dot{\gamma}_0 = 5.000(10^2)/s$$
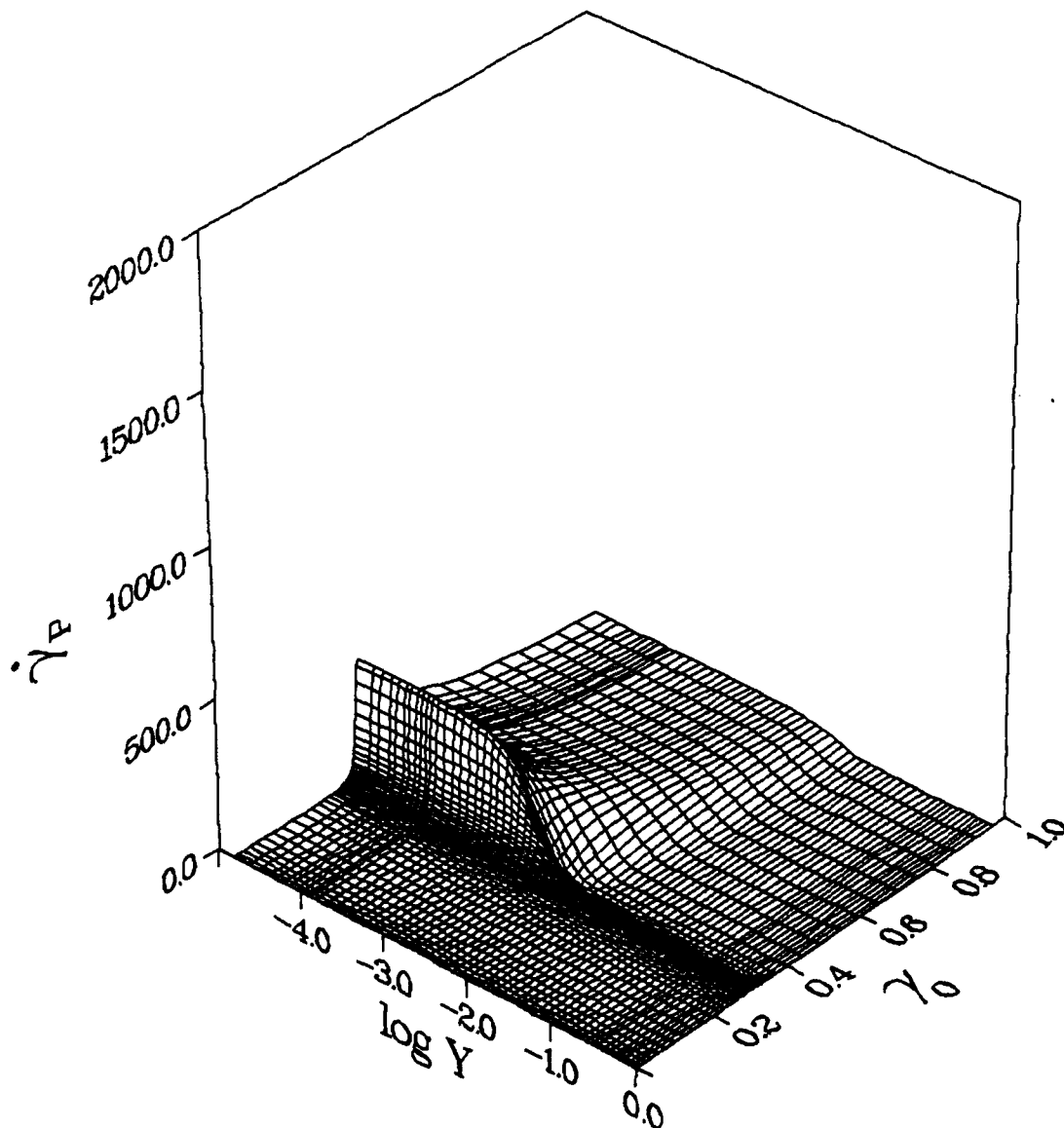
Figure 5. Plastic Strain Rate Surface at $\dot{\gamma}_o$ = 500/s for Softening Variant g_4.

$\dot{\gamma}_0 = 5.000(10)^2/s \quad Y = 0.000(10)^0$

$\dot{\gamma}_0$

$g(\theta)$

$(1-a\theta/.9)^{.9}$

$(1-a\theta)$

$\exp(-a\theta)$

$.5(1+\exp(-2a\theta))$

$\dot{\gamma}_p$

0.20   0.25   0.30   0.35

0.0   500.0   1000.0   1500.0   2000.0
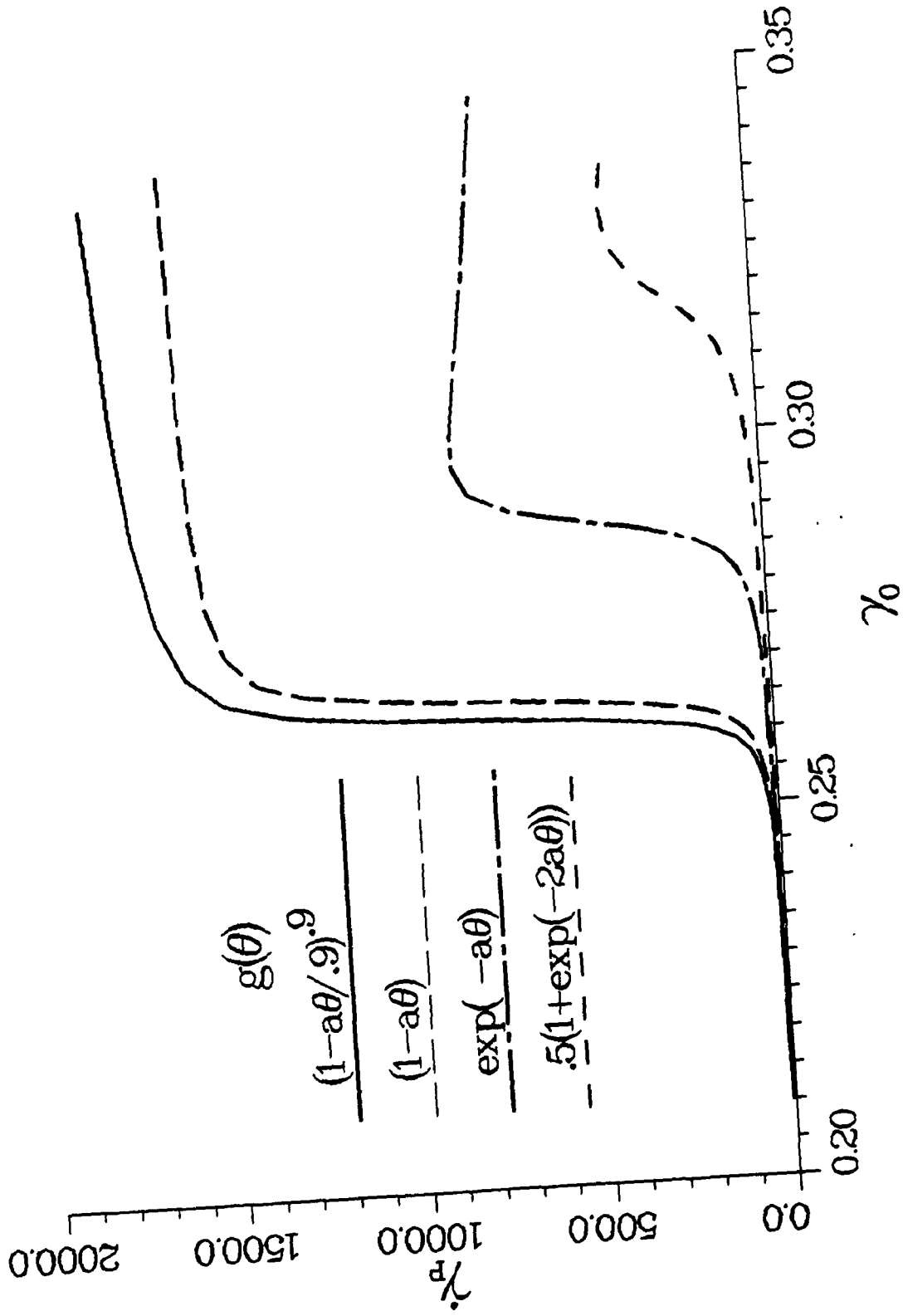
Figure 6. Plastic Strain Rate at $\dot{\gamma}_0 = 500/s$ and $\gamma = 0$ for Softening Variants g_1-g_4.

39
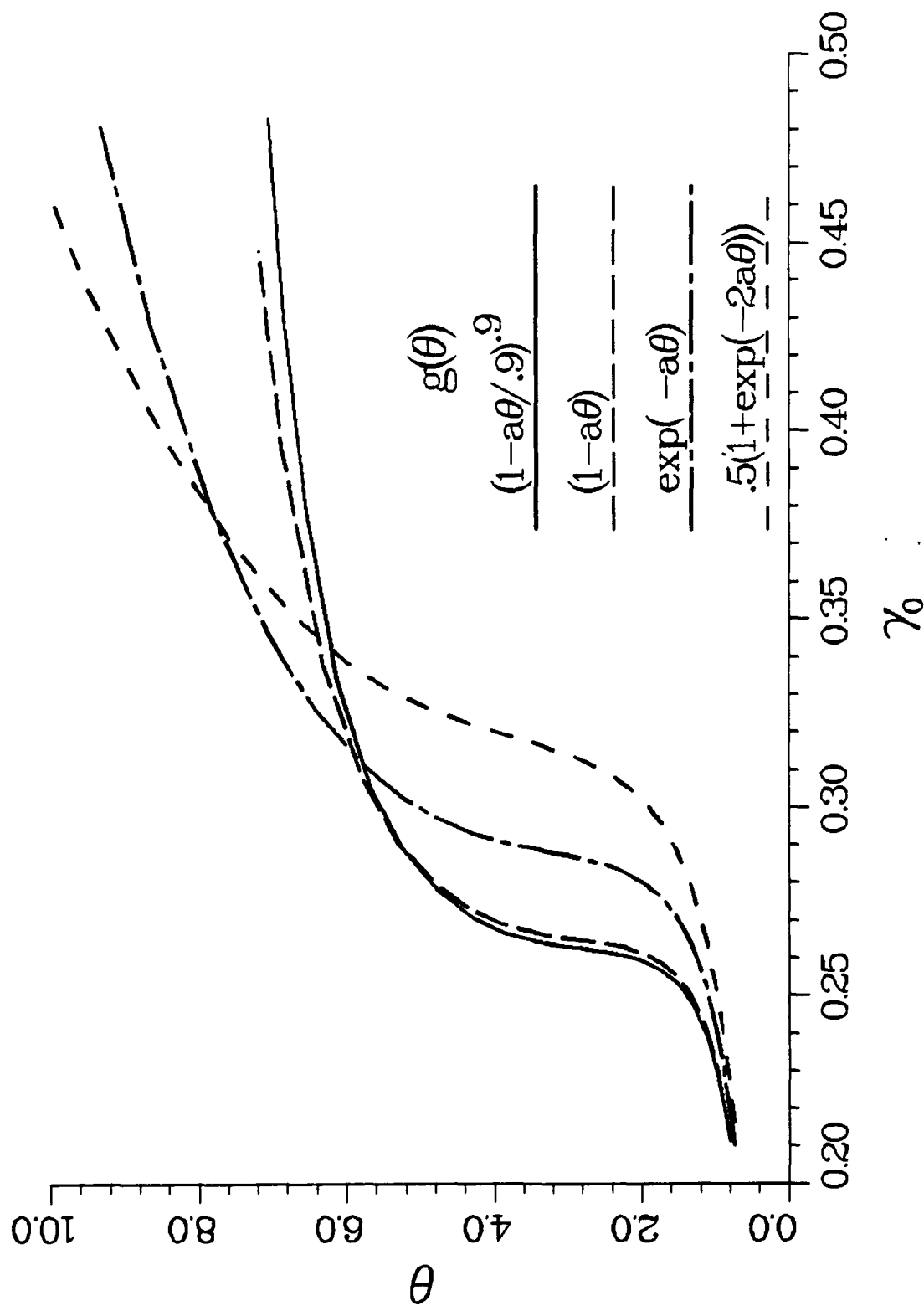
Figure 7. **Temperature at $\dot{\gamma}_0 = 500/s$ and $y = 0$ for Softening Variants g_1–g_4.**

$\dot{\gamma}_0 = 5.000(10)^2/s \quad Y = 0.000(10)^0$

$g(\theta)$

$(1-a\theta/.9)^{.9}$

$(1-a\theta)$

$\exp(-a\theta)$

$.5(1+\exp(-2a\theta))$
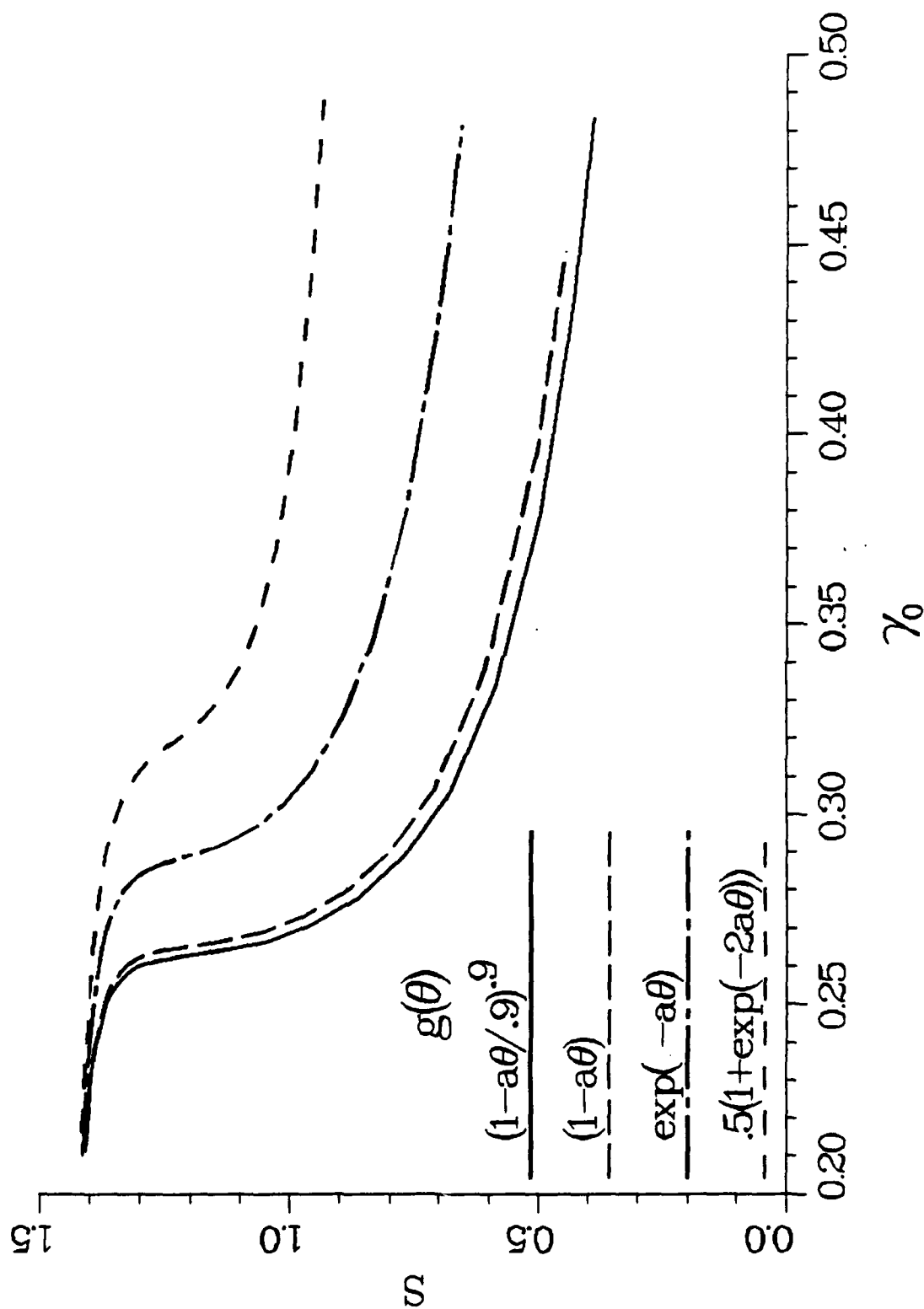
Figure 8. Stress at $\dot{\gamma}_0 = 500/s$ and $y = 0$ for Softening Variants $g_1 - g_4$.

$$\dot{\gamma}_0 = 5.000(10)^{\,2}/s \quad \gamma_0 = 5.000(10)^{-1}$$

$g(\theta)$

$(1-a\theta/.9)^{.9}$

$(1-a\theta)$

$\exp(-a\theta)$

$.5(1+\exp(-2a\theta))$

Y

W_P
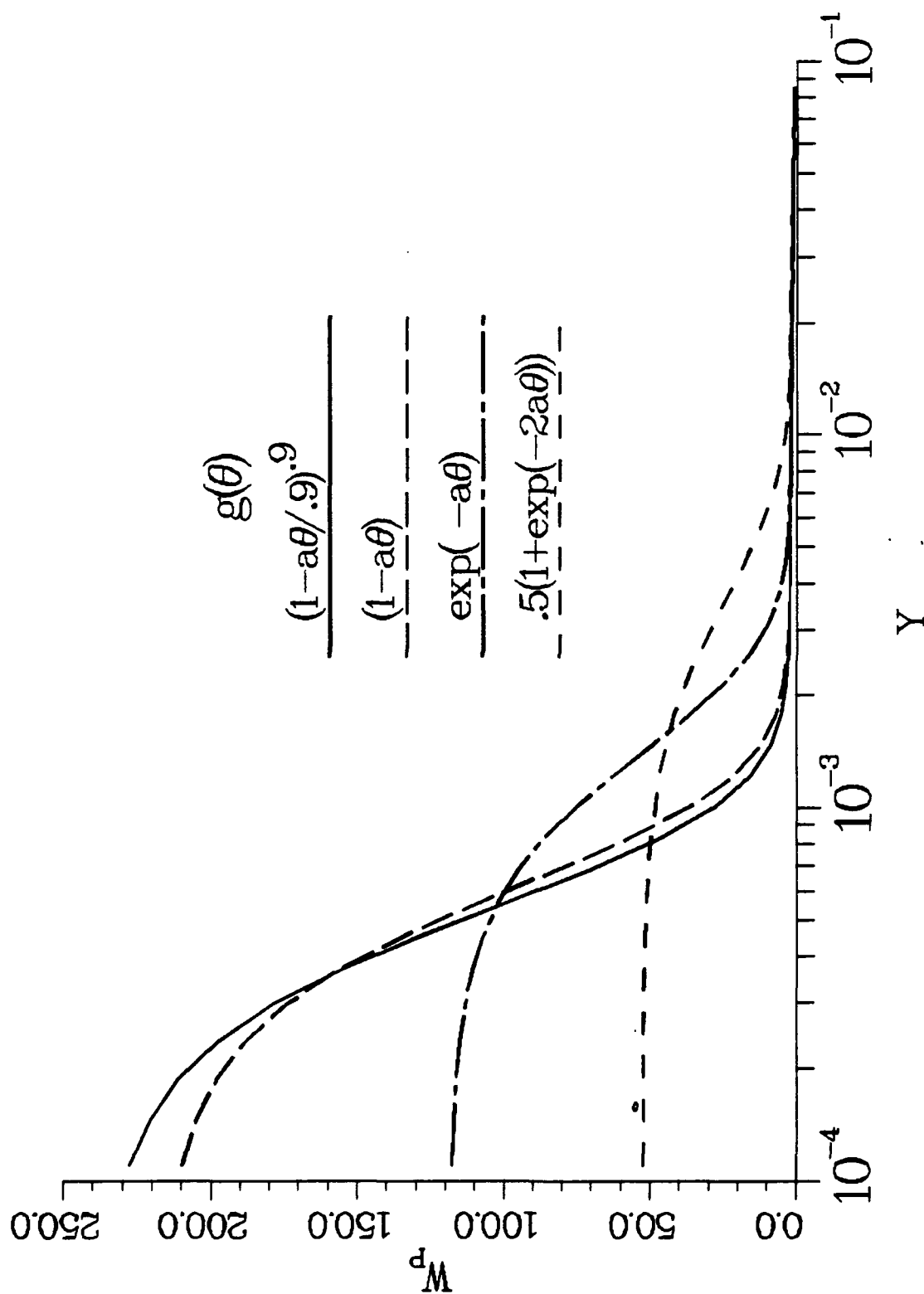
Figure 9. Plastic Work at $\dot{\gamma}_o = 500/s$ and $\gamma_o = 0$ for Softening Variants g_1–g_4.

$\dot{\gamma}_0 = 5.000(10)^2/s \quad \gamma_0 = 5.000(10)^{-1}$

g(θ)

$\dfrac{(1-a\theta/.9)^{.9}}{}$

$(1-a\theta)$

$\exp(-a\theta)$

$.5(1+\exp(-2a\theta))$
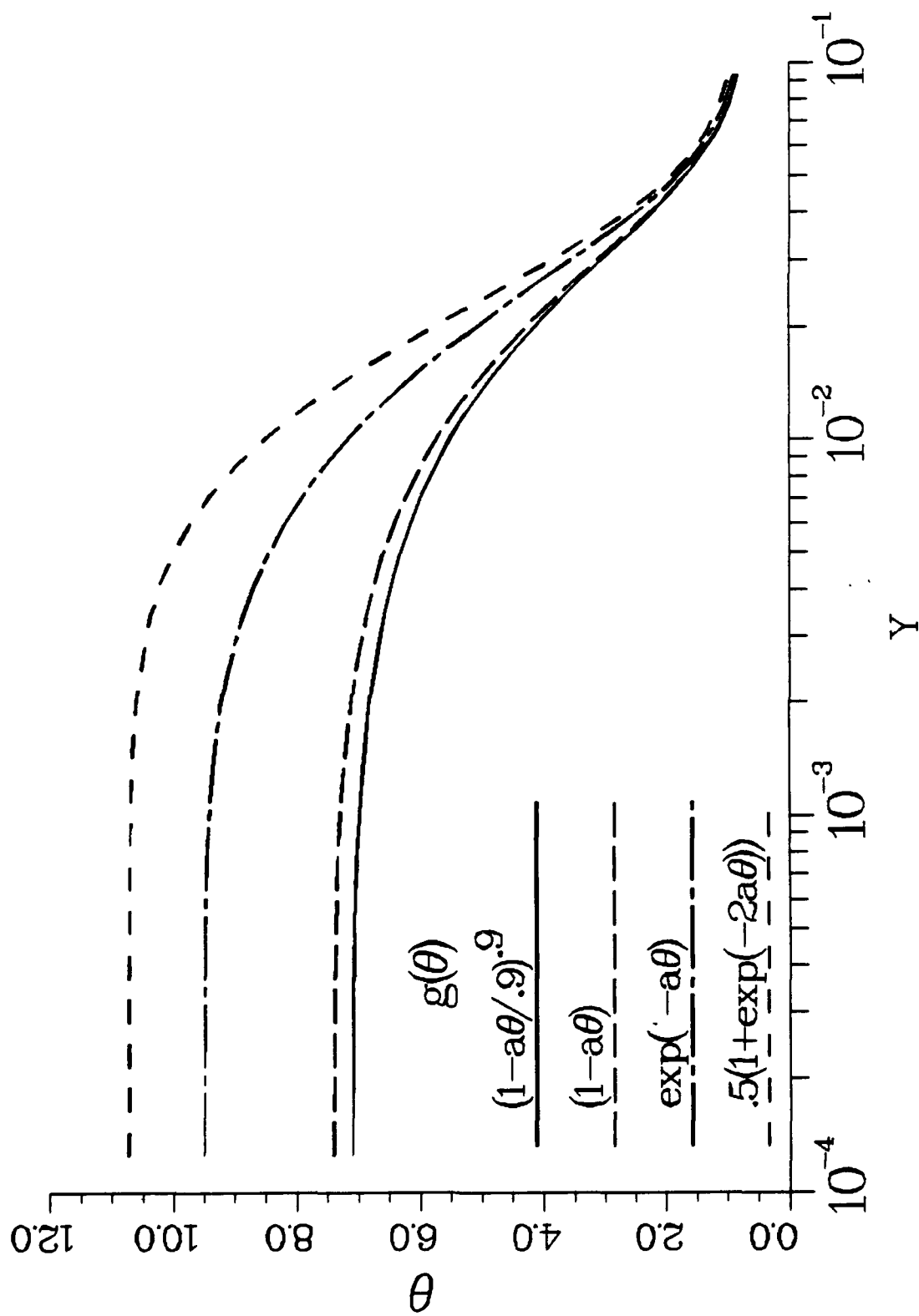
Figure 10. Temperature at $\dot{\bar{\gamma}}_o$ = 500/s and $\bar{\gamma}_o$ = 0.5 for Softening Variants g_1–g_4.

43
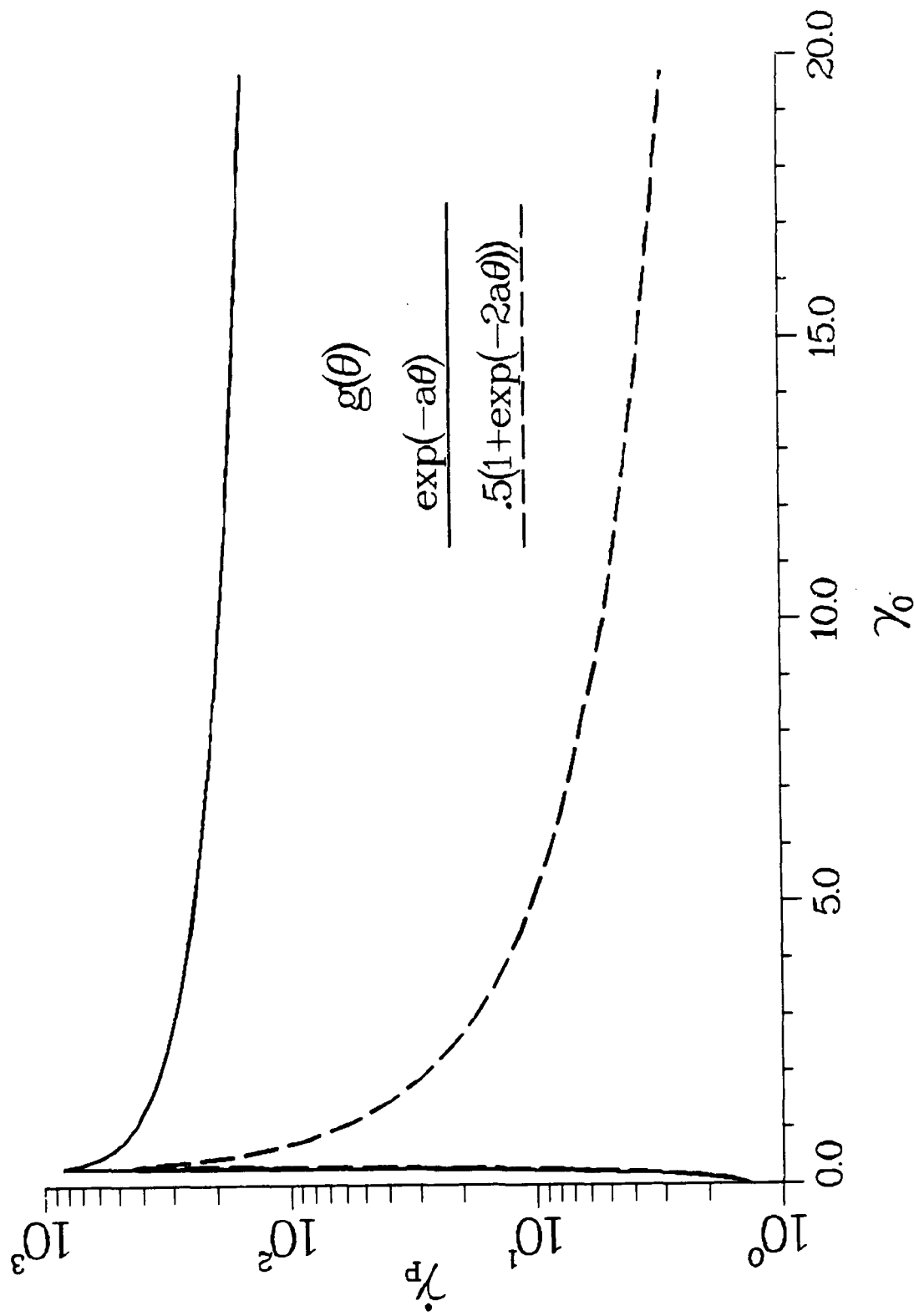
Figure 11. Plastic Strain Rate at $\dot{\bar{\gamma}}_0 = 500/s$ and $y = 0$ at Large Nominal Strains for Softening Variants g_3 and g_4.

44
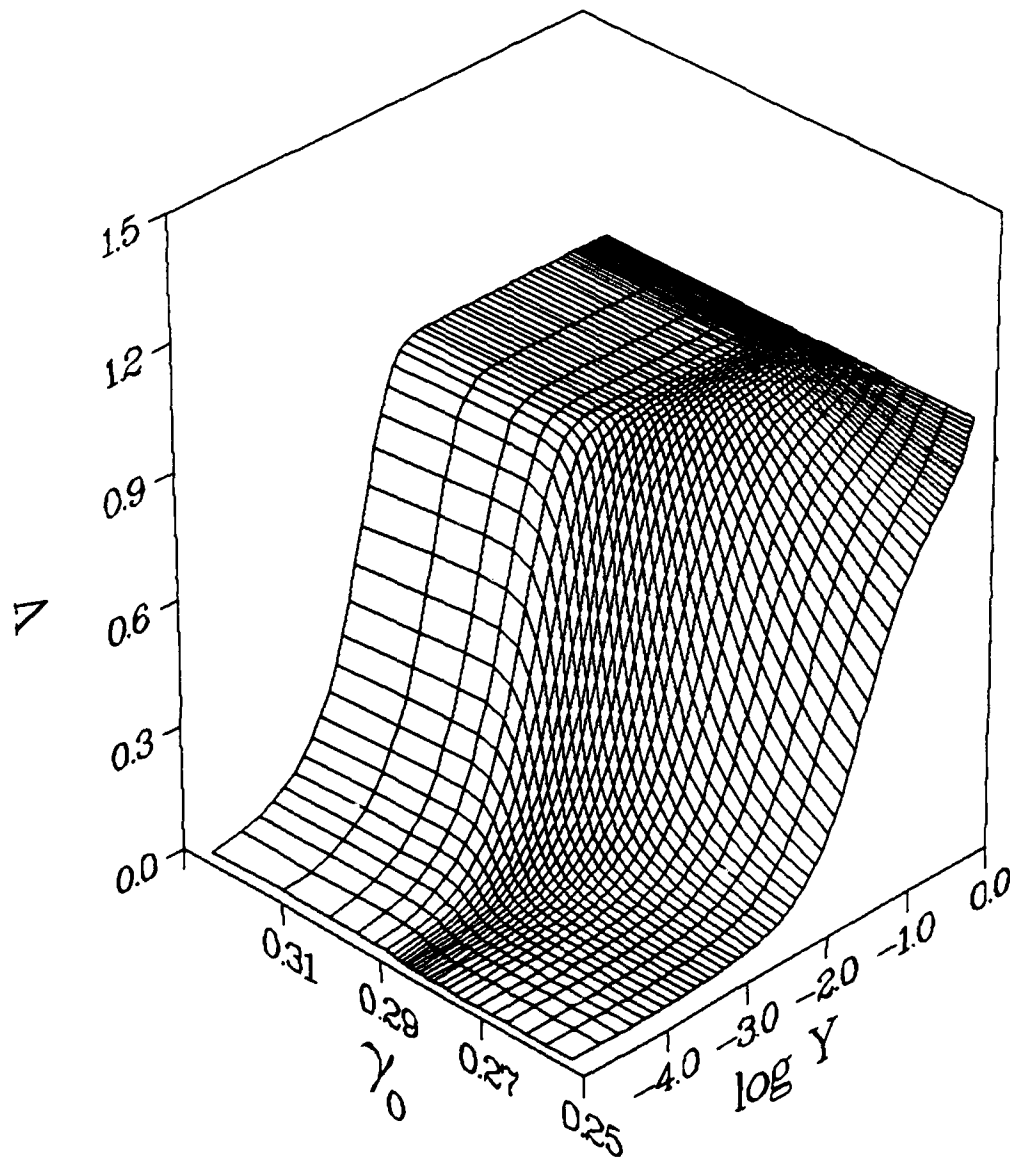
$$\dot{\gamma}_0 = 5.000(10^2)/s$$

Figure 12. Velocity Surface at $\dot{\gamma}_o$ = 500/s for Softening Variant g_3 and the Rigid, Perfectly Plastic Flow Law.

$$\dot{\gamma}_0 = 5.000(10^2)/s$$
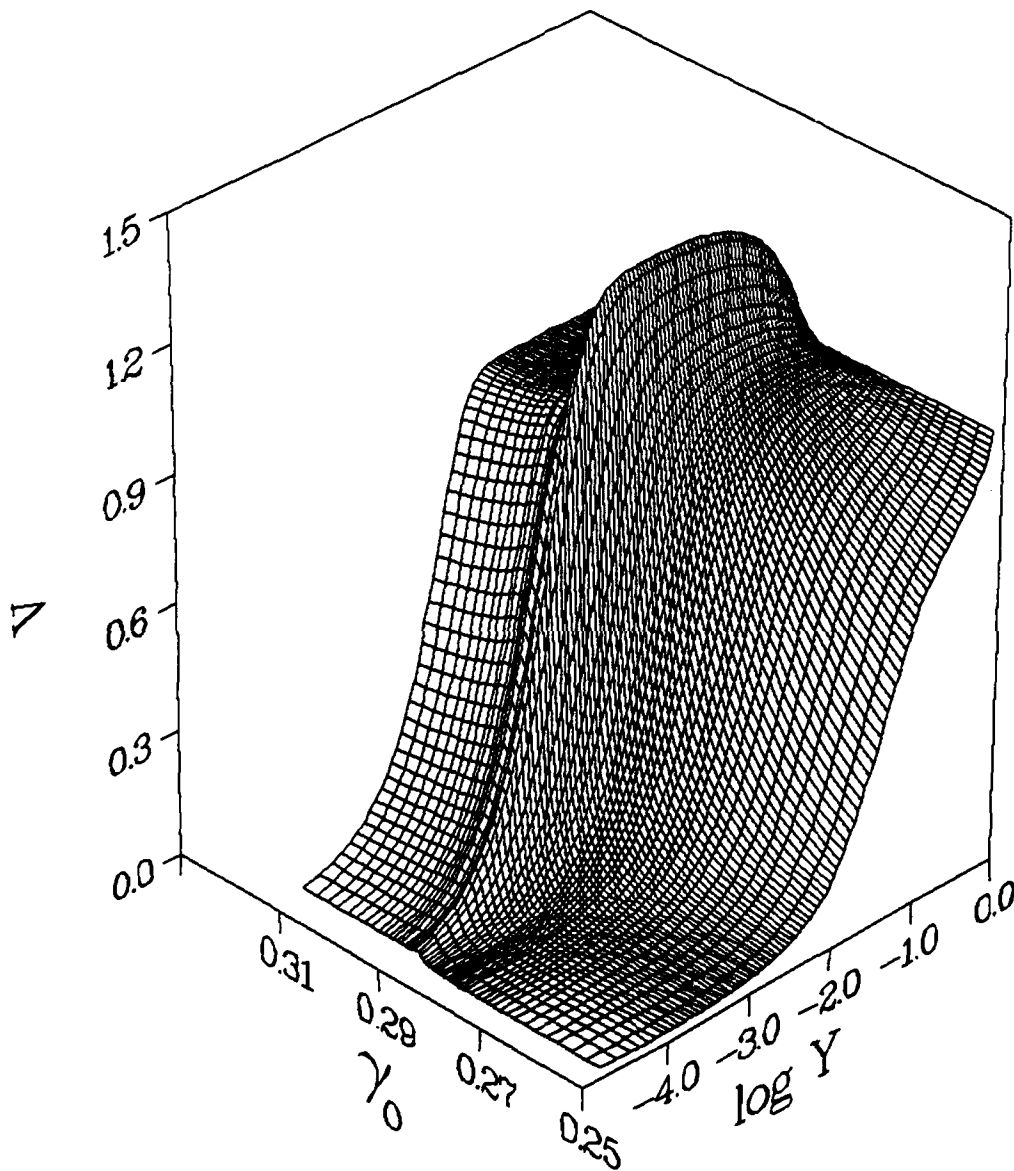
Figure 13. Velocity Surface at $\dot{\gamma}_0$ = 500/s for Softening Variant g_s and the Elastic, Perfectly Plastic Flow Law.

46
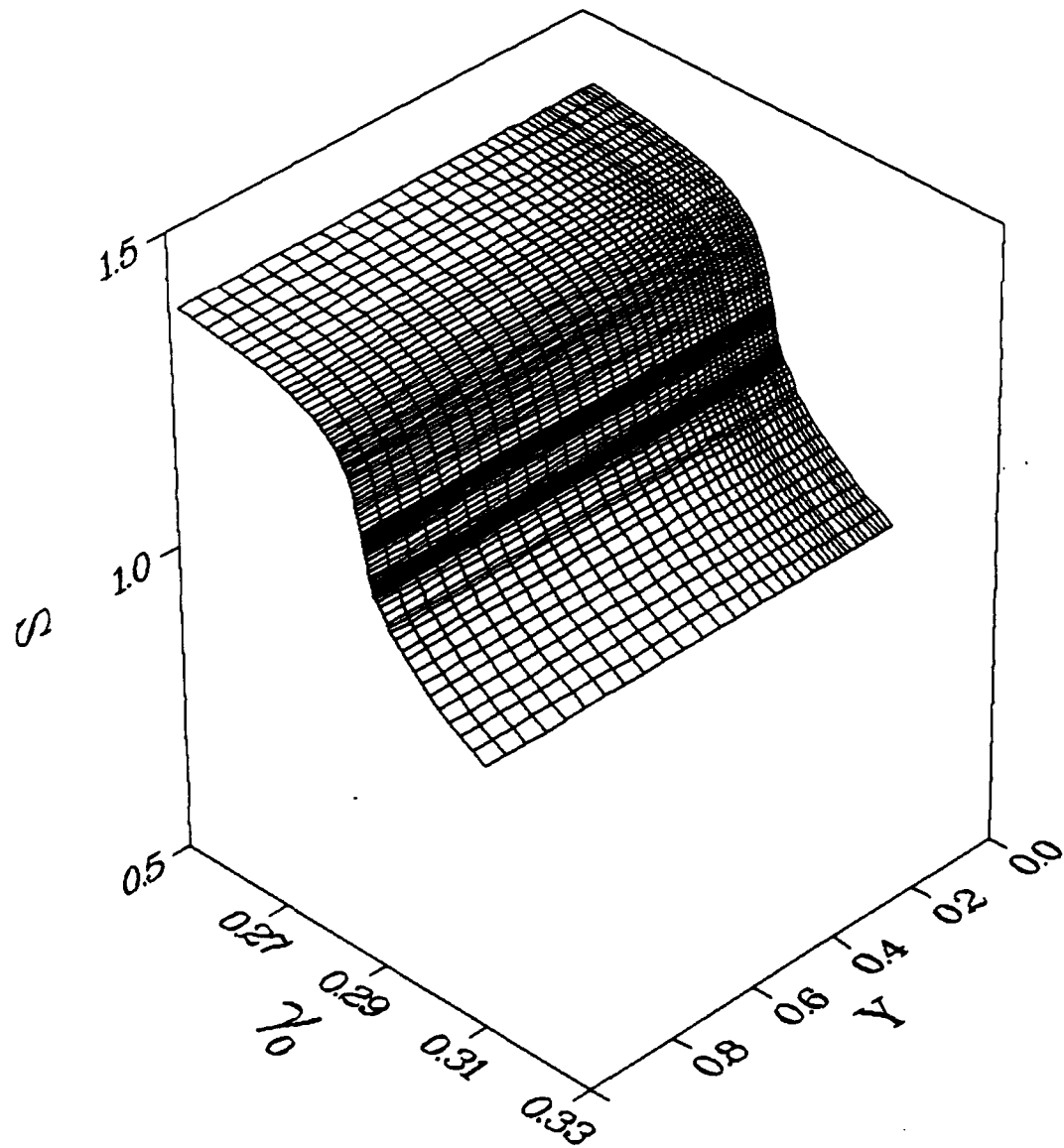
$$\dot{\gamma}_0 = 5.000(10^2)/s$$

Figure 14. Stress Surface for the Case of Figure 13.
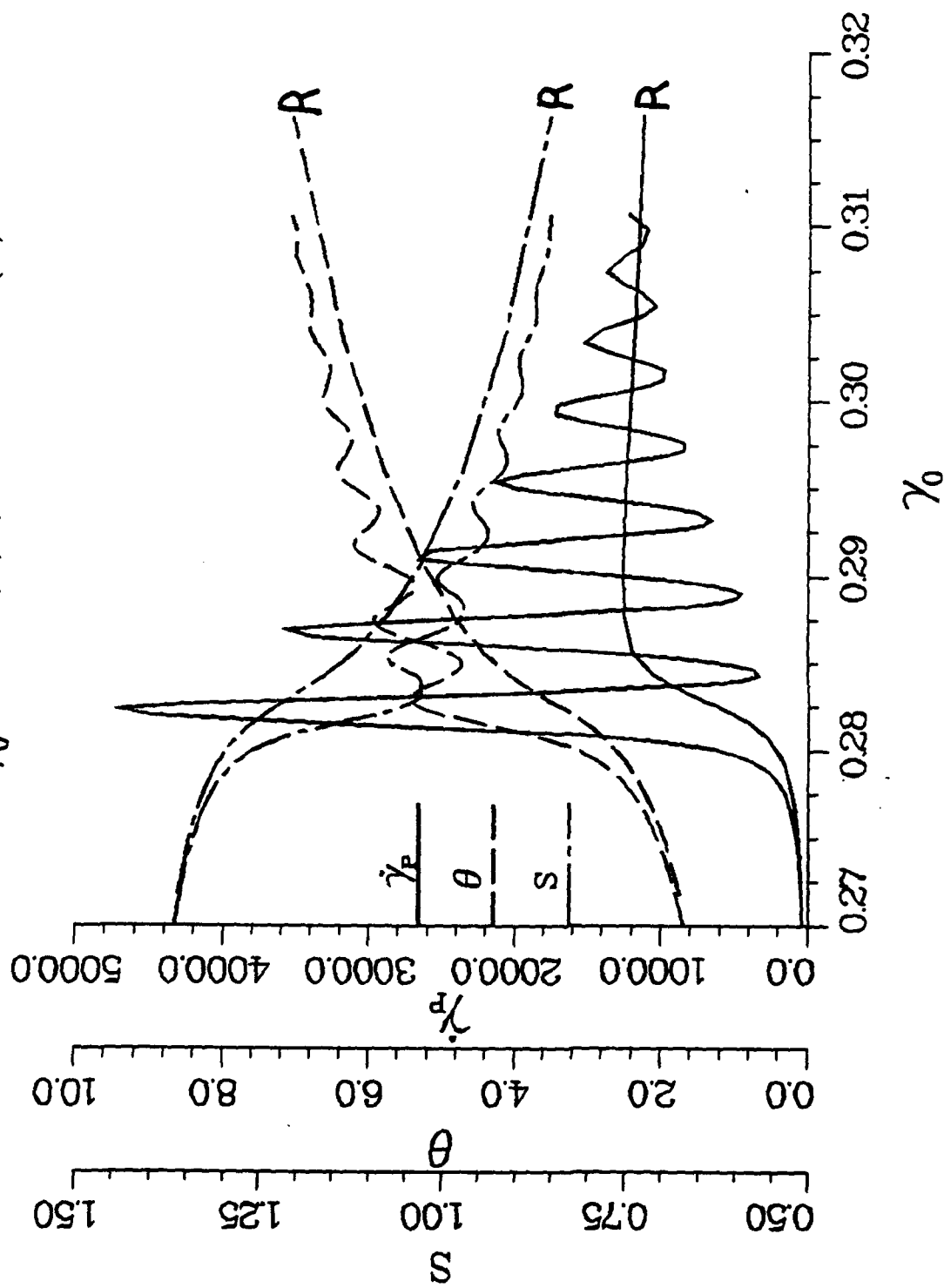
Note: The latter curves are marked with an "R".

Figure 15. Plastic Strain Rate, Temperature, and Stress at $y = 0$ for the Case of Figure 13 Superimposed on Curves for the Corresponding Rigid Case.

48

$\dot{\gamma}_0 = 5.000(10)^2/s \quad Y = 0.000(10)^0$
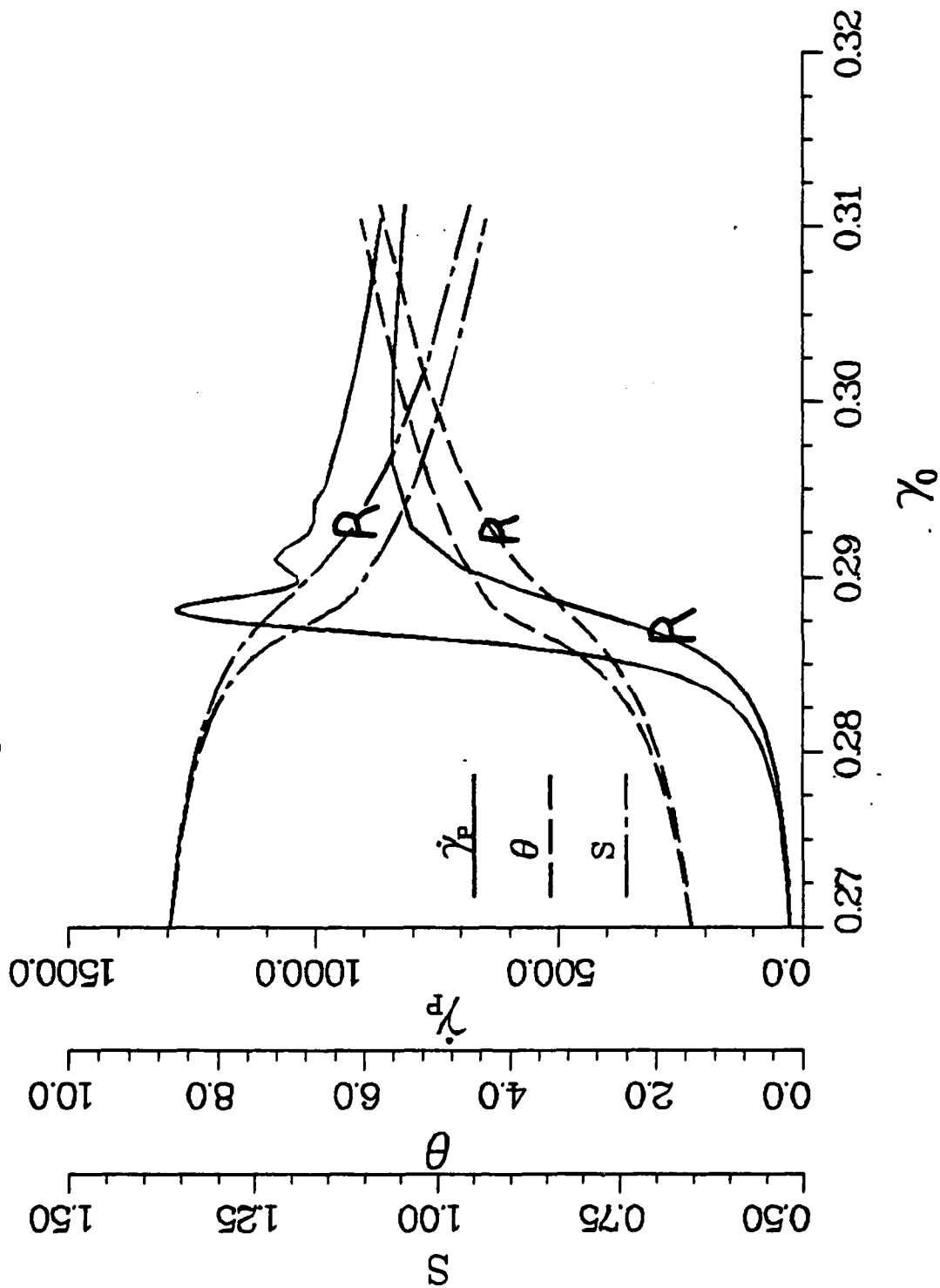
Note: Curves in the corresponding ($\dot{\gamma}_o = 750/s$) rigid case are superimposed and marked with an "R".

Figure 16. Plastic Strain Rate, Temperature, and Stress at $y = 0$ and $\dot{\gamma}_o = 750/s$ for the Elastic Material Model as in Figure 13.
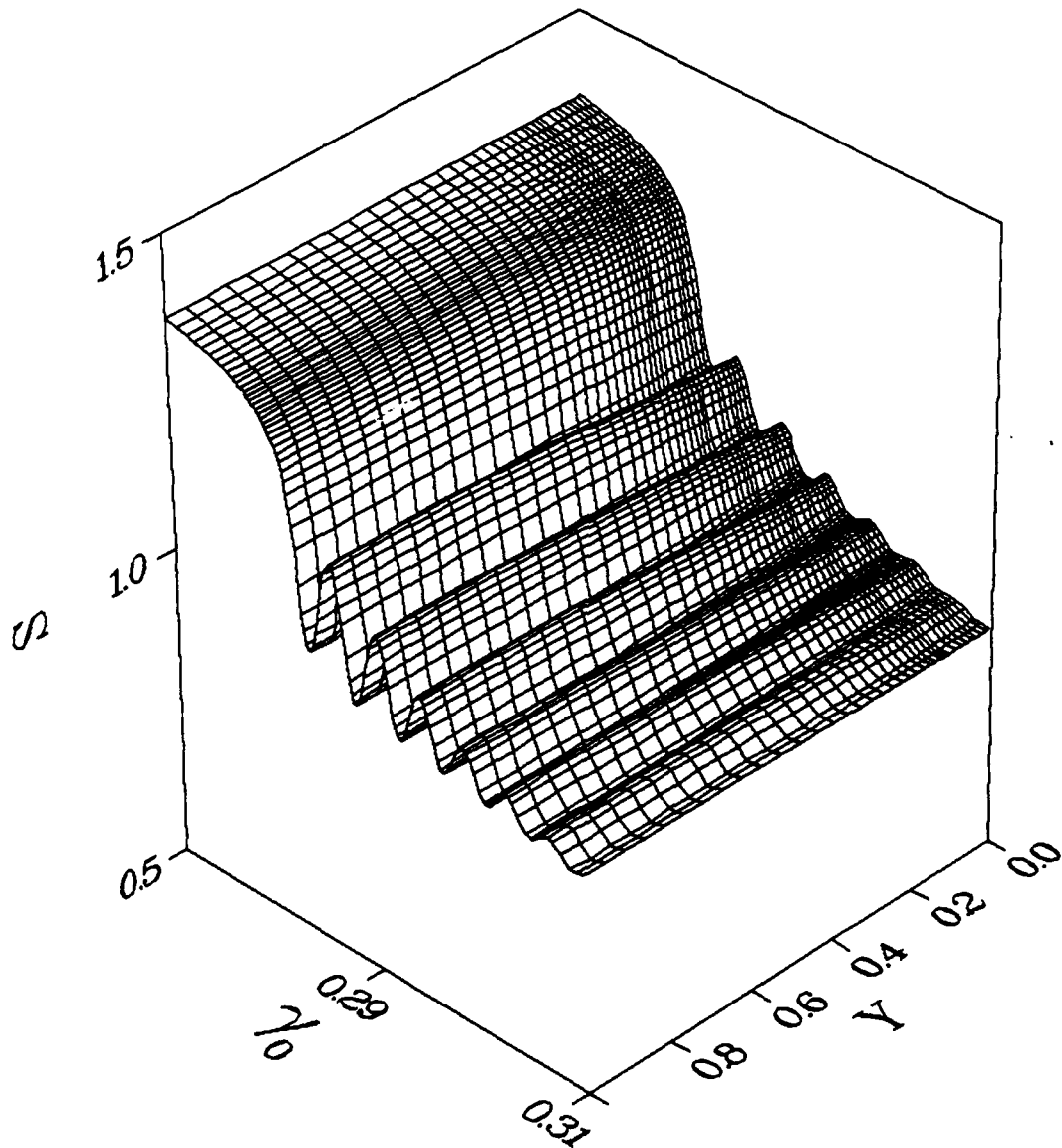
$$\dot{\gamma}_0 = 7.500(10^2)/s$$

Figure 17. <u>Stress Surface for the Case of Figure 16</u>.

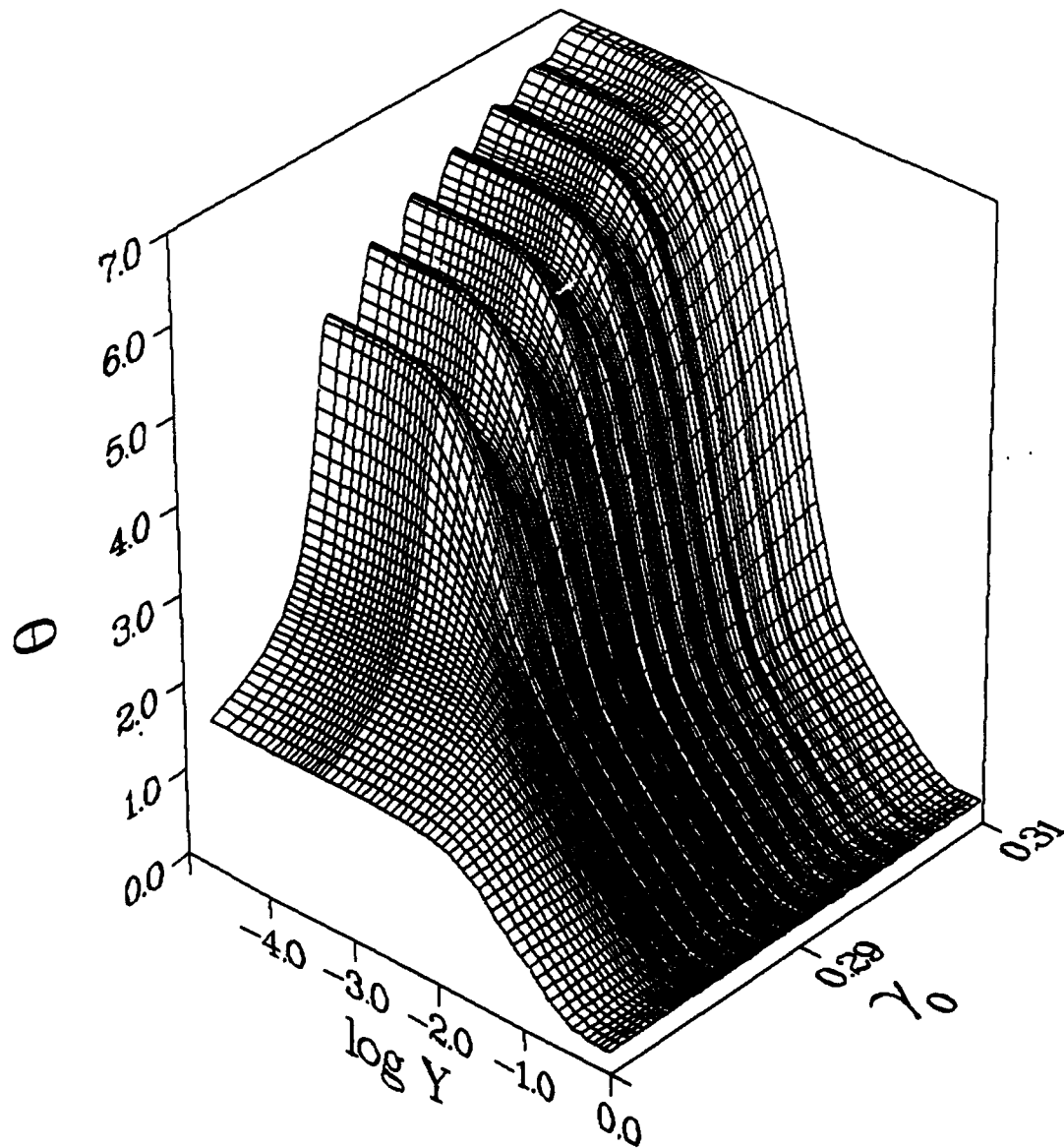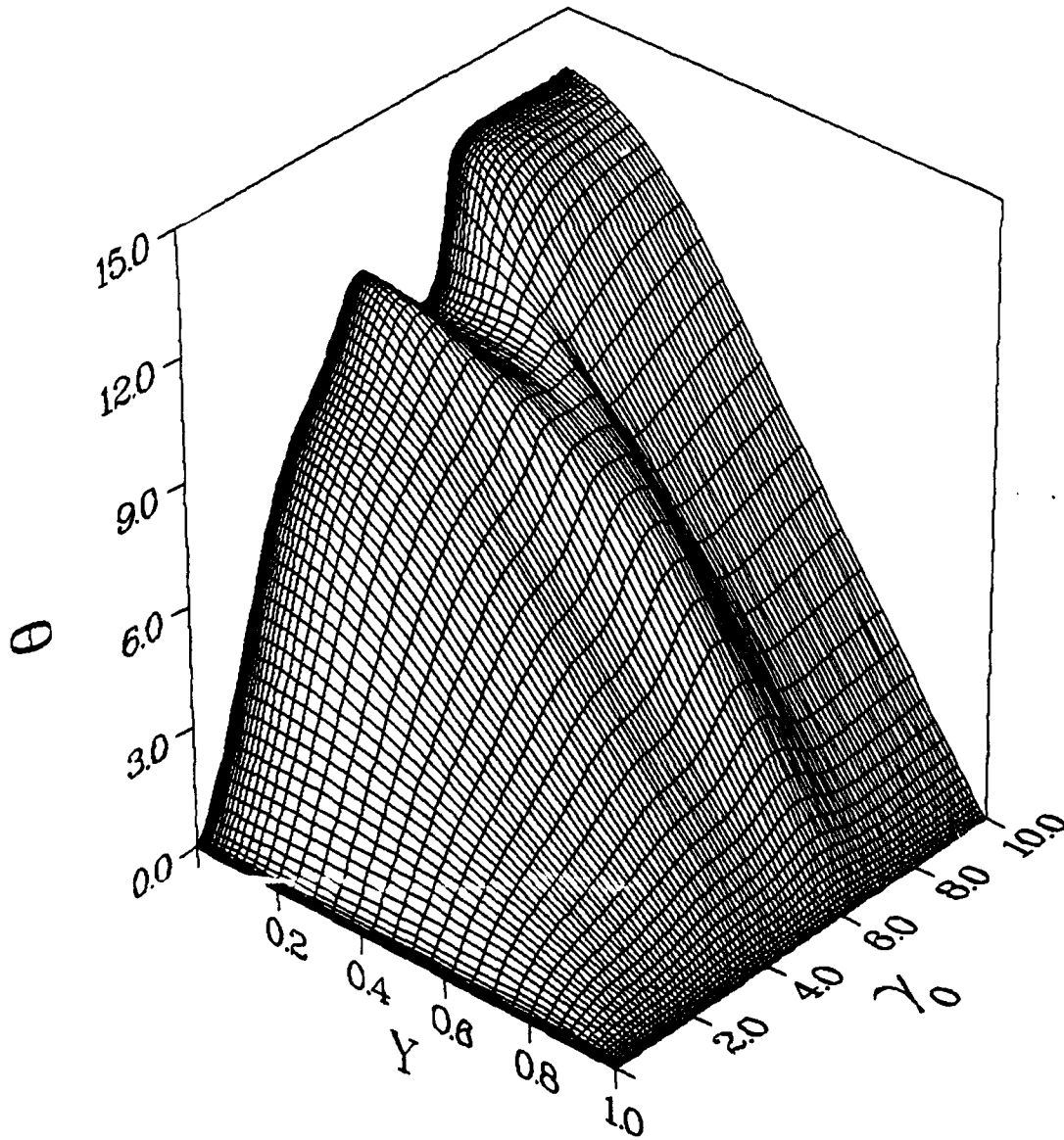$$\dot{\gamma}_0 = 7.500(10^2)/s$$

Figure 18. Temperature Surface for the Case of Figure 16.

$$\dot{\gamma}_0 = 3.300(10^2)/s$$

Note the Linear y-Axis Scale.

Figure 19.   Temperature at $\dot{\gamma}_o$ = 330/s for the Material Model as in Section 4.3 and Table 4.
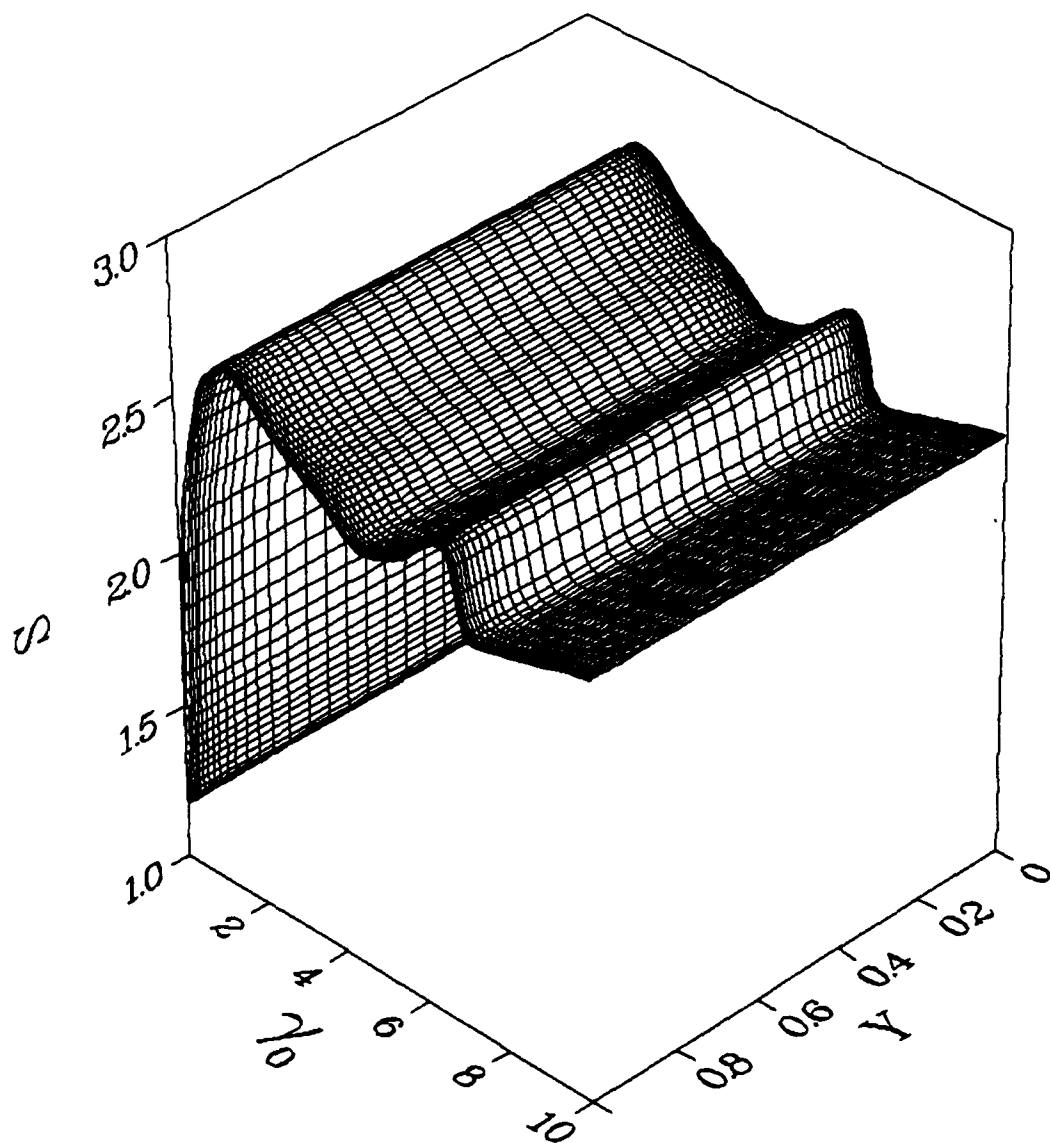
$$\dot{\gamma}_0 = 3.300(10^2)/s$$

Figure 20. Stress at $\dot{\gamma}_o = 330/s$ for the Case of Figure 19.
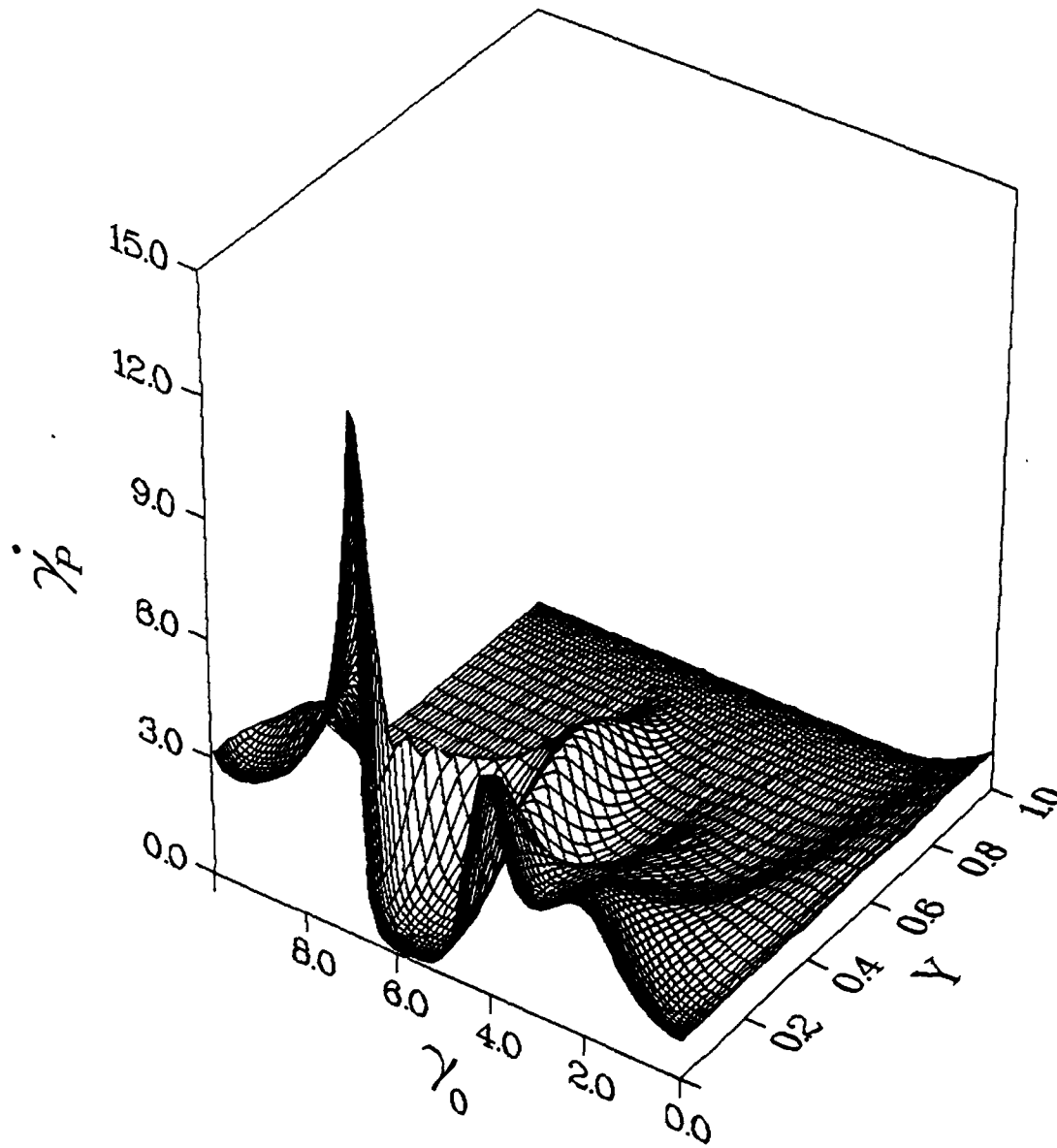
$$\dot{\gamma}_0 = 3.300(10^2)/s$$

Figure 21. Plastic Strain Rate at $\dot{\gamma}_o$ = 330/s for the Case of Figure 19.

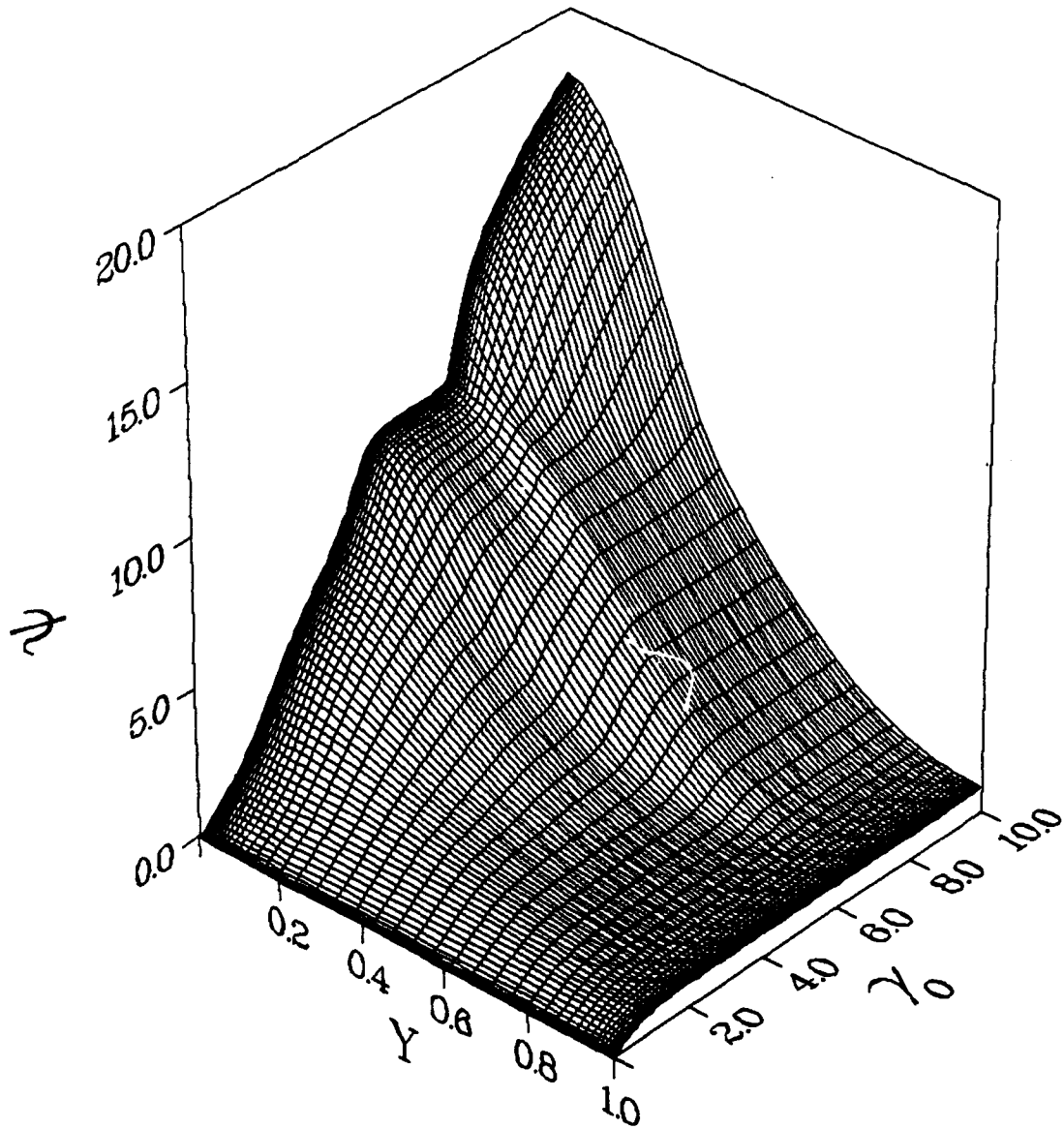$$\dot{\gamma}_0 = 3.300(10^2)/s$$

Figure 22. Strain Hardening Variable at $\dot{\gamma}_0 = 330/s$ for the Case of Figure 19.

Figure 23. $\dot{\gamma}_p$, θ, s, ψ at $y = 0$ for the Case of Figure 19.

56
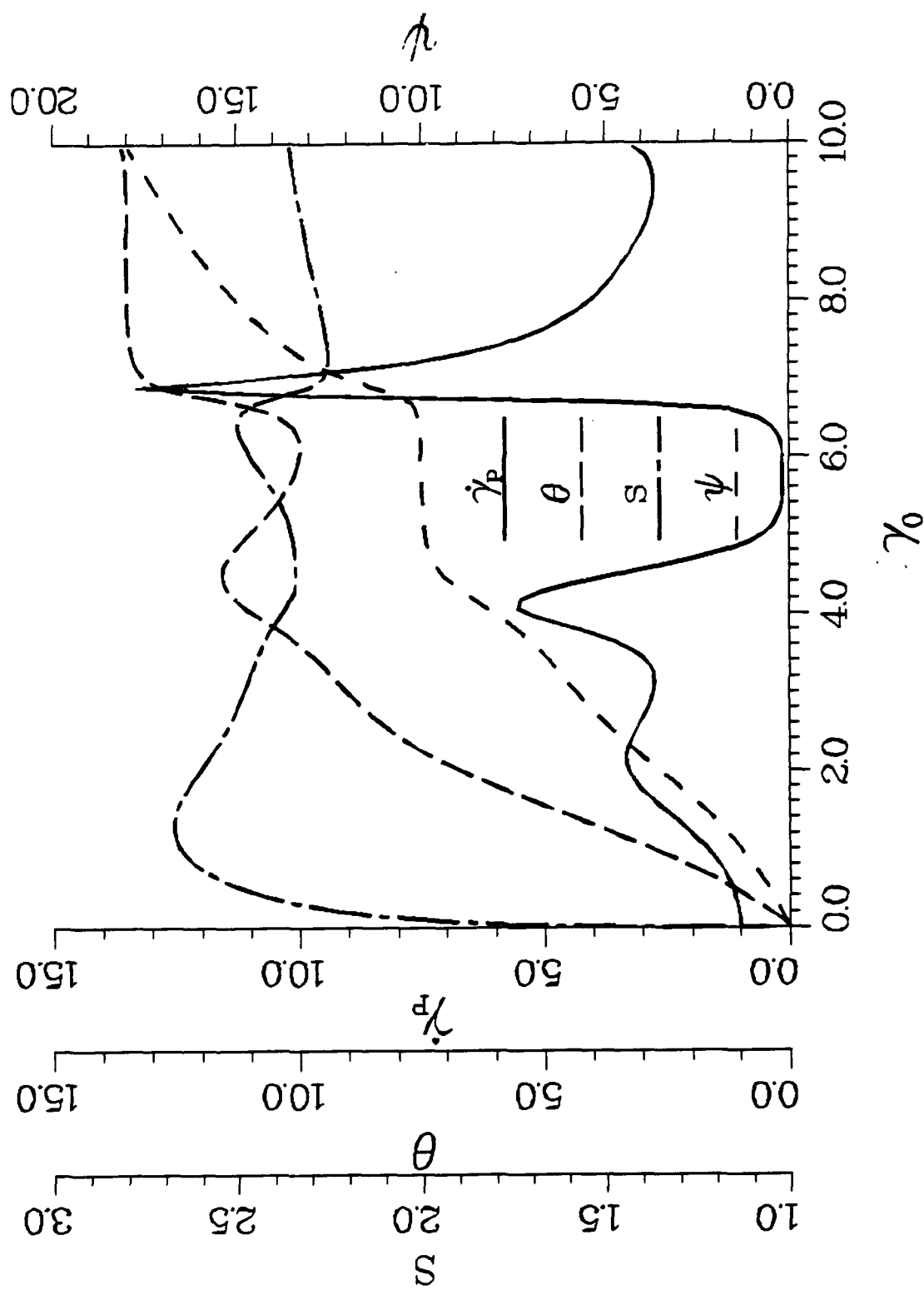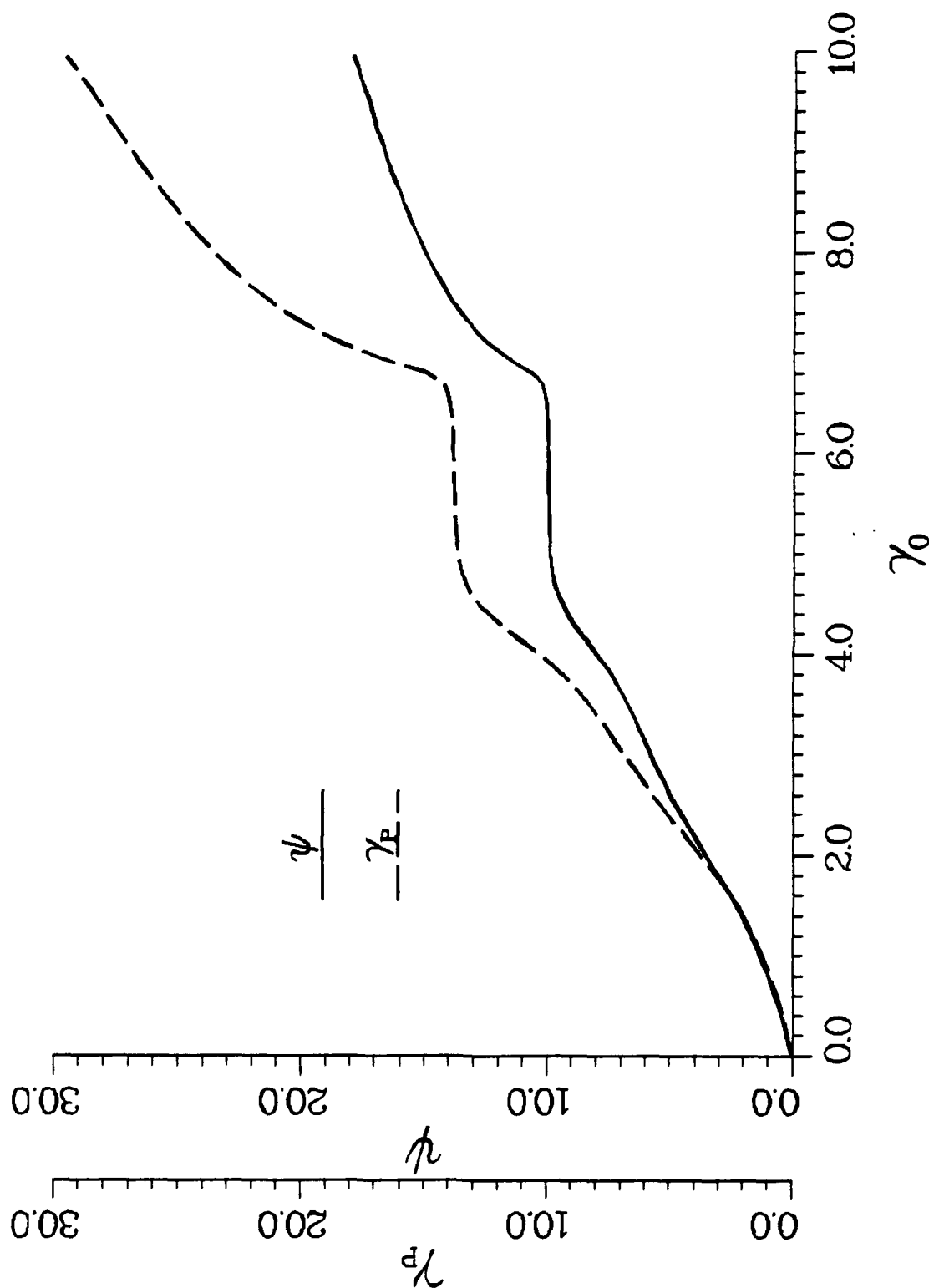
Figure 24. Strain Hardening Variable and Equivalent Plastic Strain at $y = 0$ for the Case of Figure 19.
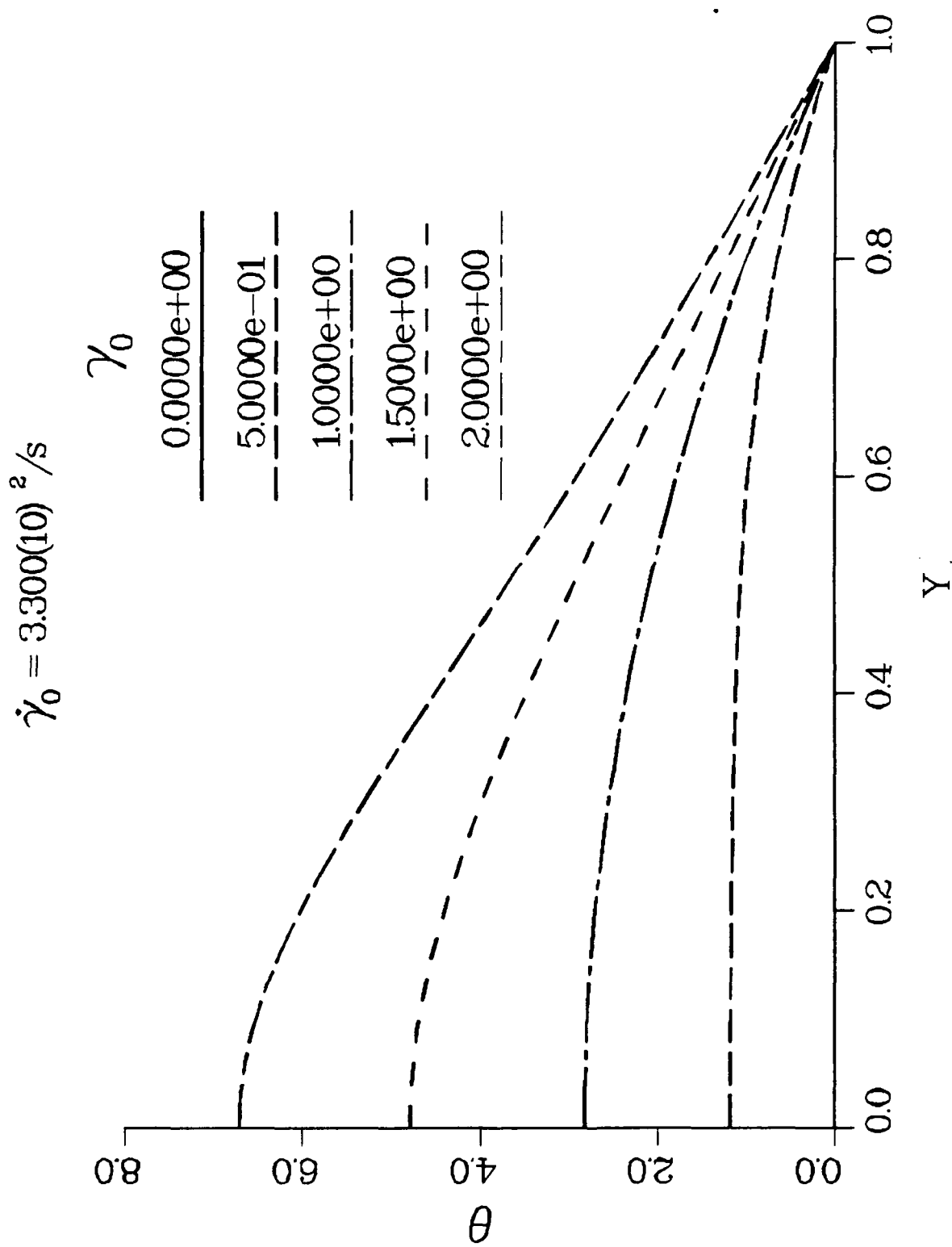
Figure 25. Temperature Profiles at Several Times During Thermal Boundary Layer Propagation for the Case of Figure 19.
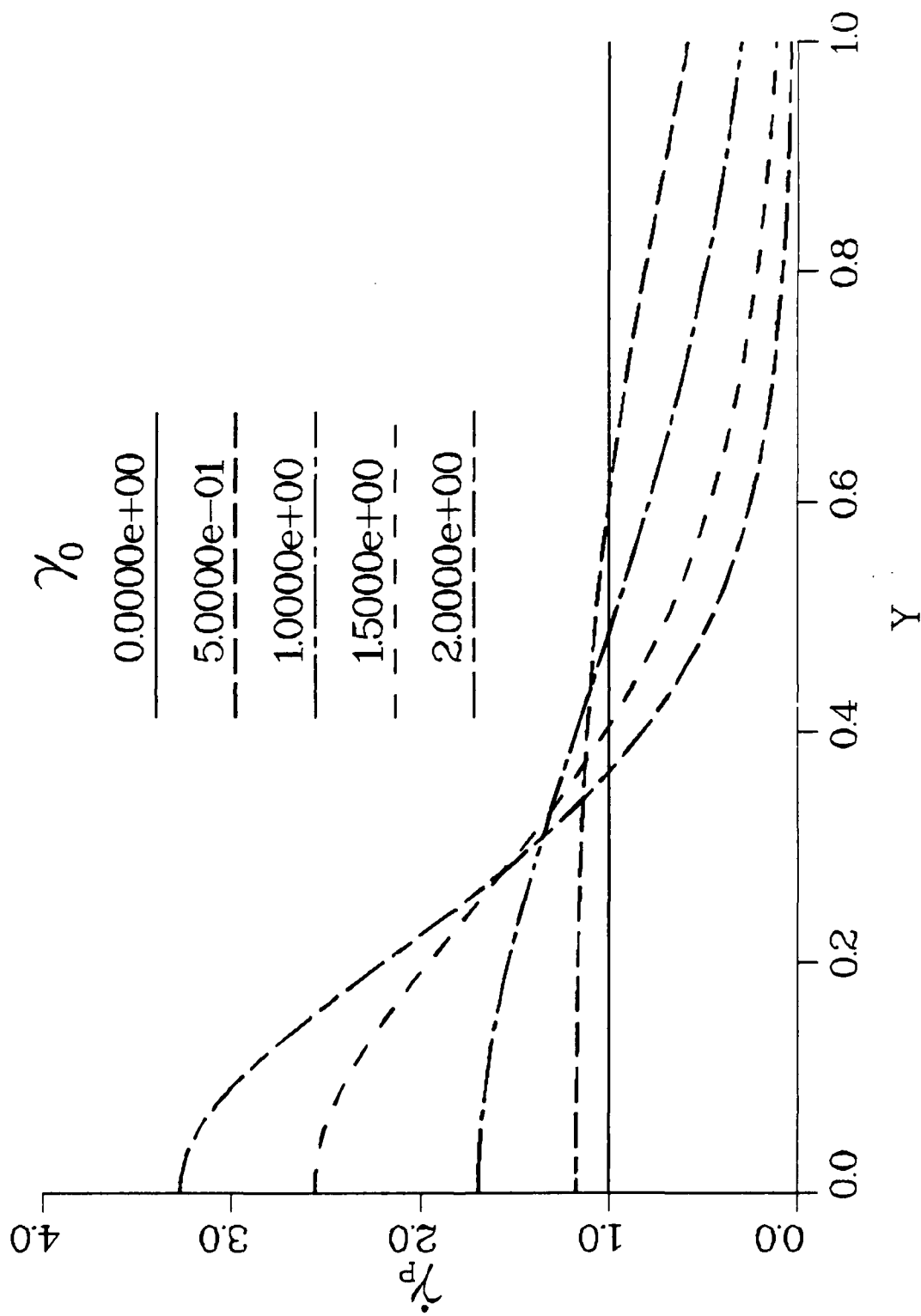
Figure 26. Plastic Strain Rate Profiles at Several Times During Thermal Boundary Layer Propagation for the Case of Figure 19.

INTENTIONALLY LEFT BLANK.

APPENDIX:

NUMERICAL METHOD

INTENTIONALLY LEFT BLANK.

We employ a semidiscrete Galerkin finite element method (Becker et al. 1981) which is based upon a weak spatial formulation of the field equations (Equation [15]). In view of the dissipation introduced by heat conduction, we shall assume that smooth and bounded initial/boundary data will *not* lead to solutions which develop singularities in finite time. In particular, we assume that at each time t any solution, $u(\cdot,t) = [\upsilon(\cdot,t),\theta(\cdot,t),s(\cdot,t),\psi(\cdot,t)]$, lies in the Sobolev space

$$H^1([0,1]) = \left\{ u{:}[0,1] \to \mathbb{R}^4 \,\middle|\, ||u||^2 = \int_0^1 [u(y)\cdot u(y) + u_y(y)\cdot u_y(y)]\,dy < \infty \right\},$$

and is smooth enough so that all the integrals appearing in the variational formulation below are finite. The specifics of the weak formulation also depend, of course, on the boundary conditions. For example, if we augment Equations (15) and (19) with

$$\upsilon(1,t) = V(t), \quad k\theta_y(1,t) = Q(t), \tag{A-1}$$

where V and Q are the velocity and heat flux imposed at the outer boundary, and use trial and test functions from H^1, then there follows a:

Variational Formulation. *At each time $t > 0$, determine functions $\upsilon \,\varepsilon\, v_t([0,1])$ and $\theta,s,\psi \,\varepsilon\, H^1([0,1])$ such that,*

$$\int_o^1 \dot{\upsilon}a\,dy = -\;-(1/\rho)\int_o^1 sa_y\,dy, \quad \text{for all } a \,\varepsilon\, H_o^1, \tag{A-2}$$

$$\int_o^1 \dot{\theta}b\,dy = -k\int_o^1 \theta_y b_y\,dy + \int_o^1 s\dot{\gamma}_p b\,dy + Q(t)b(1), \quad \text{for all } b \,\varepsilon\, H^1, \tag{A-3}$$

$$\int_o^1 \dot{s}c\,dy = -\mu\int_o^1 [\upsilon c_y + \dot{\gamma}_p c]\,dy + \mu V(t)c(1), \quad \text{for all } c \,\varepsilon\, H^1, \tag{A-4}$$

$$\int_o^1 \dot{\psi}d\,dy = \int_o^1 (s\dot{\gamma}_p/\kappa)d\,dy, \quad \text{for all } d \,\varepsilon\, H^1, \tag{A-5}$$

63

where

$$\upsilon_t = \{a \in H^1 \mid a(0) = 0, \, a(1) = V(t)\}$$

and

$$H_o^1 = \{a \in H^1 \mid a(0) = 0, \, a(1) = 0\}.$$

Since only first order spatial gradients of the trial and test functions appear in Equations (A-5)–(A-5), it follows that a minimal finite element approximation is obtained by using piecewise, linear global basis functions (*ibid*). Assuming N nodes, the resulting system of nonlinear, first-order, ordinary differential equations for the nodal unknowns $\{\upsilon_i, \theta_i, s_i, \psi_i\}(t)$ may be written as

$$\tilde{M}_{ij}\dot{\upsilon}_j = -\rho^{-1}\tilde{D}_{ij}s_j, \quad M_{ij}\dot{\theta}_j = -kH_{ij}\theta_j + P_{ij}s_j + \delta_{iN}Q(t), \tag{A-6}$$

$$M_{ij}\dot{s}_j = -\mu(D_{ij}\upsilon_j + w_i - \delta_{iN}V(t)), \quad M_{ij}\psi_j = Z_{ij}s_j. \tag{A-7}$$

Here, δ_{ij} indicates the Kronecker delta, i varies from 1 to N, repeated indices are summed over this range, a superposed tilde indicates that all elements of row and column 1 and N of the matrix have been set to 0, and

$$M_{ij} = \int_o^1 \phi_i\phi_j \, dy, \quad D_{ij} = \int_o^1 \phi_{i,y}\phi_j \, dy, \quad H_{ij} = \int_o^1 \phi_{i,y}\phi_{jy} \, dy, \tag{A-8}$$

$$P_{ij} = \int_o^1 \dot{\gamma}_p\phi_i\phi_j \, dy, \quad Z_{ij} = \int_o^1 (\dot{\gamma}_p/\kappa)\phi_i\phi_j \, dy, \quad w_i = \int_o^1 \dot{\gamma}_p\phi_i \, dy, \tag{A-9}$$

in which ϕ_i is the global basis function for the ith node. The discrete forms of the initial conditions at $t = 0$ are obtained simply as

$$\upsilon_i(0) = \upsilon(y_i, 0), \quad i = 1, \cdots, N,$$

where $\upsilon(y,0)$ is the initial value of the velocity and similarly for $\{\theta_i, s_i, \psi_i\}$. The integrals are evaluated element-wise using two-point Gauss quadrature which is exact for the terms in

64

Equation (A-8). As it is inconvenient to implement a Dirichlet boundary condition such as Equation (19)₁ directly, a penalty method is used instead (*ibid*). Lastly, to avoid ill-conditioning of Equations (A-6) and (A-7), which may occur because a highly nonuniform mesh is required to resolve the large gradients which occur during shear band formation, each row is scaled by its diagonal element so that

$$M_{ij} = 1, \quad i = 1, \cdots, N \quad \text{no sum on } i).$$

Application of the finite element method has reduced the original IBVP to an initial value problem for which a variety of numerical methods of solution are available. However, the kinetics of shear band formation render this system numerically *stiff* and use of an appropriate method is essential if reasonable efficiency is to be obtained.[*] The work of Gear (1971), among others, has led to the development of sophisticated algorithms for the integration of such systems based on backward difference formulae and the particular package employed here is the LSODES code written by Hindmarsh (1983) as part of the Lawrence Livermore ODEPACK library. This implementation of the Gear method features a variable time step and variable order, backward difference formulae which are controlled automatically in order to satisfy a step-wise error criterion.

The full system of nodal equations in assembled form may be written

$$M\dot{w} = f(w) \quad \text{or} \quad \dot{w} = M^{-1} f(w), \tag{A-10}$$

where $w = (v_1, \theta_1, s_1, \psi_1, \cdots, v_N, \theta_N, s_N, \psi_N)$. LSODES requires the explicit form of the system (Equation [A-10]₂) and some approximation of the Jacobian, $J = M^{-1} \partial f / \partial w$, which is treated internally as a general sparse matrix. To determine the sparsity structure of J, we observe that since $M = M^T$ is diagonally dominant (only the fourth subdiagonal is nonzero), it follows that M^{-1} is also diagonally dominant and all but every fourth subdiagonal is identically zero. As $\partial f / \partial w$ is banded, it follows that J is diagonally dominant (although not banded).

---

[*]Roughly speaking, a system of ordinary differential equations is numerically stiff if, when conditionally stable integration methods are used, the maximum "acceptable" time step is governed by the *stability* of the method rather than by its *accuracy*.

To exploit this structure, the shear band code used allows the user to specify the width of a band inside of which only nonzero elements of J are stored, and outside of which all elements of J are treated as zero. Although algorithms for sparse matrices incur more computational overhead than those for full or banded matrices, the reduction in floating point operations and constitutive function evaluations appears to outweigh this overhead and so yield improved computational efficiency. For the calculations reported in the sequel, the J-bandwidth used corresponds to 20 elements, although using 10 elements usually produced identical results.

No. of Copies	Organization
2	Administrator Defense Technical Info Center ATTN: DTIC-DDA Cameron Station Alexandria, VA 22304-6145
1	Commander U.S. Army Materiel Command ATTN: AMCAM 5001 Eisenhower Ave. Alexandria, VA 22333-0001
1	Commander U.S. Army Laboratory Command ATTN: AMSLC-DL 2800 Powder Mill Rd. Adelphi, MD 20783-1145
2	Commander U.S. Army Armament Research, Development, and Engineering Center ATTN: SMCAR-IMI-I Picatinny Arsenal, NJ 07806-5000
2	Commander U.S. Army Armament Research, Development, and Engineering Center ATTN: SMCAR-TDC Picatinny Arsenal, NJ 07806-5000
1	Director Benet Weapons Laboratory U.S. Army Armament Research, Development, and Engineering Center ATTN: SMCAR-CCB-TL Watervliet, NY 12189-4050
(Unclass. only)1	Commander U.S. Army Rock Island Arsenal ATTN: SMCRI-TL/Technical Library Rock Island, IL 61299-5000
1	Director U.S. Army Aviation Research and Technology Activity ATTN: SAVRT-R (Library) M/S 219-3 Ames Research Center Moffett Field, CA 94035-1000
1	Commander U.S. Army Missile Command ATTN: AMSMI-RD-CS-R (DOC) Redstone Arsenal, AL 35898-5010

No. of Copies	Organization
1	Commander U.S. Army Tank-Automotive Command ATTN: ASQNC-TAC-DIT (Technical Information Center) Warren, MI 48397-5000
1	Director U.S. Army TRADOC Analysis Command ATTN: ATRC-WSR White Sands Missile Range, NM 88002-5502
1	Commandant U.S. Army Field Artillery School ATTN: ATSF-CSI Ft. Sill, OK 73503-5000
(Class. only)1	Commandant U.S. Army Infantry School ATTN: ATSH-CD (Security Mgr.) Fort Benning, GA 31905-5660
(Unclass. only)1	Commandant U.S. Army Infantry School ATTN: ATSH-CD-CSO-OR Fort Benning, GA 31905-5660
1	WL/MNOI Eglin AFB, FL 32542-5000

Aberdeen Proving Ground

No. of Copies	Organization
2	Dir, USAMSAA ATTN: AMXSY-D AMXSY-MP, H. Cohen
1	Cdr, USATECOM ATTN: AMSTE-TC
3	Cdr, CRDEC, AMCCOM ATTN: SMCCR-RSP-A SMCCR-MU SMCCR-MSI
1	Dir, VLAMO ATTN: AMSLC-VL-D
10	Dir, USABRL ATTN: SLCBR-DD-T

No. of
Copies Organization

4   Brown University
    Division of Engineering
    ATTN: R. Clifton
            J. Duffy
            B. Freund
            A. Needleman
    Providence, RI 02912

1   Brown University
    Division of Applied Mathematics
    ATTN: C. Dafermos
    Providence, RI 02912

5   University of California at
        San Diego
    Dept. of Applied Mechanics and
        Engineering Sciences
    ATTN: R. Asaro
            G. Hegemeier
            X. Markenscoff
            M. Meyers
            S. Nemat-Nasser
    La Jolla, CA 92093

3   California Institute of Technology
    ATTN: W. Knauss
            G. Ravichandran
            A. Rosakis
    Mail Code 105-50
    Pasadena, CA 91125

1   Carnegie-Mellon University
    Dept. of Mathematics
    ATTN: M. Gurtin
    Pittsburg, PA 15213

1   University of Cincinnati
    Dept. of Mathematical Sciences
    ATTN: D. French
    Old Chemistry Bldg, ML 25
    Cincinnati, OH 45221

1   Cornell University
    Dept. of Theoretical and
        Applied Mechanics
    ATTN: J. Jenkins
    Ithaca, NY 14850

No. of
Copies Organization

1   Drexel University
    Dept. of Materials Engineering
    ATTN: H. Rogers
    Philadelphia, PA 18104

1   Harvard University
    Division of Engineering and
        Applied Physics
    ATTN: J. Hutchinson
    Cambridge, MA 02138

2   University of Illinois
    Dept. of Theoretical and
        Applied Mechanics
    ATTN: D. Carlson
            T. Shawki
    Urbana, IL 61801

1   University of Illinois at
        Chicago Circle
    Dept. of Engineering, Mechanics,
        and Metallurgy
    ATTN: T. Ting
    P.O. Box 4348
    Chicago, IL 60680

2   The Johns Hopkins University
    Dept. of Mechanical Engineering
    Latrobe Hall
    ATTN: A. Douglas
            K. Ramesh
    34th and Charles Streets
    Baltimore, MD 21218

1   University of Kentucky
    Dept. of Engineering Mechanics
    ATTN: O. Dillon, Jr.
    Lexington, KY 40506

1   Lehigh University
    Center for the Application of
        Mathematics
    ATTN: E. Varley
    Bethlehem, PA 18015

2   University of Maryland
    Dept. of Mechanical Engineering
    ATTN: R. Armstrong
            J. Dally
    College Park, MD 20742

69

No. of
Copies Organization

1   Massachusetts Institute of Technology
        Dept. of Mechanical Engineering
        ATTN: L. Anand
        Cambridge, MA 02139

3   University of Minnesota
        Dept. of Aerospace Engineering
          and Mechanics
        ATTN: R. Fosdick
               R. James
               T. Tezduyar
        110 Union Street SE
        Minneapolis, MN 55455

1   University of Missouri-Rolla
        Dept. of ME, AE, and EM
        ATTN: R. Batra
        Rolla, MO 65401-0249

1   University of Nebraska
        Dept. of Engineering Mechanics
        ATTN: M. Beatty
        212 Bancroft Hall
        Lincoln, NE 68588

3   State University of New York
          at Stony Brook
        Dept. of Applied Mathematics
          and Statistics
        ATTN: J. Glimm
               J. Grove
               B. Plohr
        Stony Brook, NY 11794

1   North Carolina State University
        Dept. of Civil Engineering
        ATTN: Y. Horie
        Raleigh, NC 27607

1   North Carolina State University
        Dept. of Mathematics
        ATTN: M. Shearer
        Raleigh, NC 27695

1   North Carolina State University
        Dept. of Mechanical and
          Aerospace Engineering
        ATTN: M. Zikry
        Raleigh, NC 27695

No. of
Copies Organization

1   Northwestern University
        Dept. of Applied Mathematics
        ATTN: W. Olmstead
        Evanston, IL 60208

2   Northwestern University
        Dept. of Civil Engineering
        ATTN: T. Belytschko
               B. Moran
        Evanston, Il 60208

2   Rensselaer Polytechnic Institute
        Dept. of Mechanical Engineering
        ATTN: E. Lee
               E. Krempl
        Troy, NY 12181

2   Rensselaer Polytechnic Institute
        Dept. of Computer Science
        ATTN: J. Flaherty
               Y. Wang
        Troy, NY 12181

1   University of Texas (TICOM)
        ATTN: J. Oden
        Austin, TX 78712

1   Texas A&M University
        ATTN: T. Strouboulis
        Aerospace Engineering Dept.
        College Station, TX 77843-3141

1   Washington State University
        Dept. of Mechanical and
          Materials Engineering
        ATTN: H. Zbib
        Pullman, WA 99164

4   SRI International
        ATTN: D. Curran
               R. Shockey
               L. Seaman
               H. Giovanola
        333 Ravenswood Avenue
        Menlo Park, CA 94025

No. of
Copies Organization

3 Southwest Research Institute
  Dept. of Mechanical Sciences
  ATTN: C. Anderson
      J. Lankford
      U. Lindholm
  8500 Culebra Road
  San Antonio, TX 02912

2 Alliant Techsystems, Inc.
  ATTN: G. Johnson
      T. Holmquist
  7225 Northland Drive
  Brooklyn Park, MN 55428

2 Battelle Edgewood Operation
  ATTN: R. Jameson
      S. Golaski
  2113 Emmorton Park Rd.
  Edgewood, MD 21040

1 Institute for Advanced Technology
  ATTN: S. Bless
  4030-2 W. Braker Lane
  Austin, TX 73759-5329

No. of
Copies <u>Organization</u>

  1   Ruhr-Universitat Bochum
       ATTN: J. Kalthoff
       Universitatstrasse 150
       4360 Bochum 1, Postfach 102148
       Germany

  1   Brunel University
       Institute of Computational Mathematics
       ATTN: J. Whiteman
       Uxbridge, Middelsex
       UB8 3PH, England
       United Kingdom

USER EVALUATION SHEET/CHANGE OF ADDRESS

This Laboratory undertakes a continuing effort to improve the quality of the reports it publishes. Your comments/answers to the items/questions below will aid us in our efforts.

1. BRL Report Number ___BRL-TR-3381___ Date of Report ___July 1992___

2. Date Report Received _____

3. Does this report satisfy a need? (Comment on purpose, related project, or other area of interest for which the report will be used.) _____

_____

_____

4. Specifically, how is the report being used? (Information source, design data, procedure, source of ideas, etc.) _____

_____

_____

5. Has the information in this report led to any quantitative savings as far as man-hours or dollars saved, operating costs avoided, or efficiencies achieved, etc? If so, please elaborate. _____

_____

_____

6. General Comments. What do you think should be changed to improve future reports? (Indicate changes to organization, technical content, format, etc.) _____

_____

_____

_____

	Name
CURRENT ADDRESS	Organization
	Address
	City, State, Zip Code

7. If indicating a Change of Address or Address Correction, please provide the New or Correct Address in Block 6 above and the Old or Incorrect address below.

	Name
OLD ADDRESS	Organization
	Address
	City, State, Zip Code

(Remove this sheet, fold as indicated, staple or tape closed, and mail.)